Journal of Materials Chemistry A

Accepted Manuscript

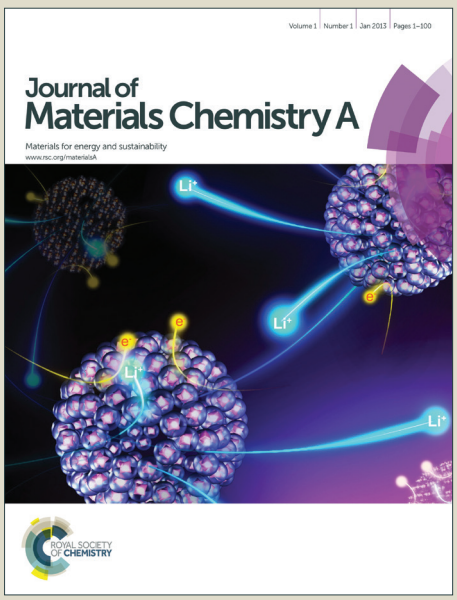

ROYAL SOCIETY OF CHEMISTRY

www.rsc.org/materialsA

Table of contents entry:

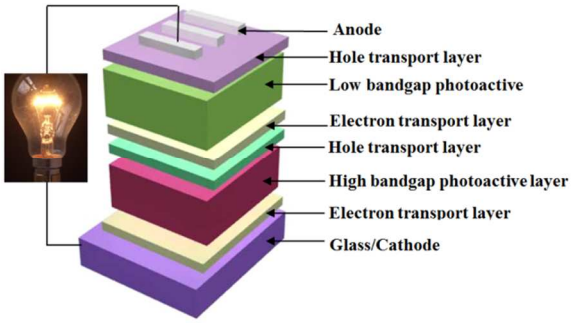

Tandem polymer solar cells can achieve significantly higher efficiencies by reducing the absorption and thermalization loss.

Double Junction Polymer Solar Cells

Olusegun Adebanjo, Bjorn Vaagensmith and Qiquan Qiao*

Received (in XXX, XXX) Xth XXXXXXXXX 20XX, Accepted Xth XXXXXXXXX 20XX

Center for Advanced Photovoltaics, Department of Electrical Engineering and Computer Sciences, South Dakota State University, Brookings, SD, 57007, USA. Tel:1-605-688-6965, Fax: 1-605-688-4401, Email:Qiquan.Qiao@sdstate.edu

Abstract

The growing need for low-cost alternative energy motivates research in polymer solar cells. To reduce the cost per watt of energy, polymer solar cells with high power conversion efficiencies are necessary. Tandem polymer solar cells can achieve significantly higher efficiencies; however there are issues associated with polymers' complementary absorption spectra, architectural designs, fabrication approaches and interfacial material selections or engineering. In this article, we review device structures: both regular and inverted architectures, efficiency estimation of double junction polymer solar cells, and the most recent progress in circumventing the limitations of tandem polymer solar cells. This article will provide the readers with insightful knowledge into developing tandem polymer solar cells with efficiencies towards 15%.

1. Introduction

Energy is central to social, human and economy development. Near-exponential population growth particularly in the 20th century resulted in 16× increment in energy demand.[1] Meanwhile, worldwide energy source supply has increased its diversity. Consumption of traditional fossil fuels is slowing down relative to historical average.[2] The shares of different primary energy sources, among which natural gas and renewables are projected to have steady increase; hydro seems constant while oil, coal, and nuclear are expected to decline beyond the year 2010.[3] Likewise, the projected contribution from renewable energy to power generation exhibited steep rise from 2010 to 2030 compared to all other sources.[3] The reduction of fossil fuel share and its harmful environmental effects from emitting CO_2 gases as well as the recent political commitments made to reduce global CO_2 gases has made renewable energy a long term attractive venture.

Solar radiation reaching the earth surface delivers approximately 89,000 TW.[4] Therefore, among all renewable energy sources solar energy is the most abundant and promising alternative with the extractable possibility of supplying more than 15 TW of power; the amount of power projected to drive a carbon-free energy source by 2050.[2]

Inorganic photovoltaics (PVs) is a matured technology having industrial and market presence and an average annual growth rate of global PV installed capacity at ~44% from 1.8 GW in 2000 to 67.4 GW in 2011.[5] Despite this fact, traditional crystalline silicon solar cells that still dominate ~90% of the global PV market remains largely unaffordable, which is majorly dependent on government subsidies. [2] This scenario explains why solar PV only accounts for paltry 0.1% of the world's electricity generation.[6] The prospect of further cost reduction increases the popularity of thin-film solar cells. Organic photovoltaic (OPV) technology have recently been attracting research and industrial attention due to that (a) absorption coefficient of organic materials is higher than inorganic counterparts leading to lower material thickness for sufficient light absorption, (b) solution-processability of organic materials such as large area roll-to-roll printing and spray coating resulting in lower cost and (c) significant progress in materials and devices engineering has led to efficiencies above 10 % in single junction OPV devices which initially was a hurdle.[7-9] All these characteristics further pave the pace towards commercialization of OPV technology.

Further OPV research and development are needed to improve device efficiency[10] and stability/lifetime[11] in order to compete favorably with inorganic PV cells. To achieve high efficiency, organic solar cells (OSCs) must have a substantial broadband absorption in the solar spectrum. Existing materials either have high absorption over a limited band of solar spectrum [12-14] or low absorption over a wide range of solar spectrum [15-18]. Materials with both high and broad absorption are still lacking. In addition, assuming a polymer exists that has broadband solar spectrum absorption, thermalization losses may become significant and decrease solar cell efficiency. One approach to achieve high absorption over a wide band of solar spectrum and reduce thermalization loss is to stack two or more solar cells with complementary absorption in a tandem configuration.[19, 20] In addition, a tandem configuration that incorporates efficient interconnecting layers eliminates the problem of high internal resistance or ineffective charge transport; a problem which arises in an attempt to increase active layer thickness to enhance absorption in single junction OSCs.[21] We wrote a review article on tandem polymer solar cells, which was published on Energy and Environmental Science in 2010.[22] From then on, significant progress in tandem polymer solar cell performance has been achieved with a world record device efficiency of 10.61% achieved by Yang group.[23] Therefore, we will provide a follow

up review focusing on the 2010-2013 period of research on tandem polymer solar cells.

This review aims to summarize the characteristics and developments of tandem polymer solar cells. First, different device geometries and roles of interlayers are discussed. Second, a chronicle of efficiency progress of tandem organic photovoltaic devices is presented. Finally, various issues that are important to tandem polymer solar cells in high-efficiency devices are highlighted.

2. Structure and efficiency estimation of double junction polymer solar cells

Tandem PSCs can provide higher power conversion efficiencies (PCEs) than single junction cells because the range of absorption spectrum can be expanded using different polymers with complementary absorption bands. In addition, donor-acceptor lowest unoccupied molecular orbitals (LUMOs) offsets in each subcell can be modified to minimize the photovotage loss. The operation of subcells in tandem PSCs is similar to single junction cells; however an inversely-oriented heterojunction between donor layer of one subcell and acceptor layer of adjacent subcell is formed if multiple subcells are serially deposited.[24] Normally, tandem PSCs with subcells deposited in series will result in build-up of space charge within the device. This situation can be prevented by inserting interlayer (recombination/tunneling layer) between adjacent subcells. The interlayer should act as a transport layer for electrons and holes; simply put, the interlayer should act as a cathode for one subcell and anode for the other subcell. The interlayer must be an efficient recombination site for opposite charge carriers from adjacent subcells. Ineffective recombination will bias individual subcells away from their maximum operating power point.[25] This recombination layer must minimize photovoltage loss by aligning the Fermi energy levels of adjacent subcells. The recombination sites can also exhibit optical spacer function in which the internal electric field of separate photoactive layers is optimized. The optical spacer effect is particularly beneficial to organic solar cells that have sufficient absorption coefficient and ~ 100-200 nm thick film limited by low charge carrier mobility.[26] Finally, the interlayer must serve as a protective layer for the underlying subcell while at the same time serve as a robust foundation for the overlying subcell. Since both subcells should have different bandgaps for effective light harvesting, it is necessary to be able to control or tune the bandgaps of conjugated polymers (especially to avoid gaps in the combined absorption spectra). Bandgap tuning of conjugated polymers can be accomplished through synthetic design of copolymerizing electron-rich (donor) and electron-deficient (acceptor) units in the polymer backbone. This 'hybrid' donor-acceptor (D-A) strategy is commonly demonstrated in low bandgap conjugated polymers because of the potential to induce bandgap compression in polymers by taking advantage of high donor HOMO and low acceptor LUMO.[27-35] Interestingly, this D-A approach has been recently used to realize wide bandgap conjugated polymers with significantly improved fill-factor (FF) and PCE.[36] Another strategy to maximize light harvesting in tandem devices is the use of certain acceptors such as fullerene derivatives to enhance absorption and compensate for unavoidable absorption gaps in donor polymers.[37] For example, when $PC_{70}BM$ was used to replace PCBM in blends with a low bandgap copolymer poly{(9,9-dioctylfluorene)-2,7-diyl-*alt*-[4,7-bis(3-decyloxythien-2-yl)-2,1,3-benzothiadiazole]-5',5"-diyl} (PF-co-DTB) that has significant absorption gaps, Yao *et al*. demonstrated an increase in device performance by 50%.[38] This enhanced performance was attributed to stronger absorption of $PC_{70}BM$ in 440-530 nm range covering the absorption gaps between two absorption peaks (416 and 584 nm) of PF-co-DTB. Recently, it had been argued that due to uncertainty in photon absorption, photoexcitation generated a delocalized long-range coherent superposition of exciton states which was against the previously and widely held belief of localized exciton generation following photon absorption process. The consequence of this startling revelation is that sometimes majority of charge carriers can be generated within ~100 fs which is sufficiently long enough to affect charge transfer dynamics. [39] Once exciton dissociation occurs at the donor-acceptor (D/A) interface, electrons and holes from adjacent subcells recombine at the interlayer of a tandem architecture while the remaining carriers are collected at the electrode. In a series-connected tandem configuration, it is important to optimize the current generated by each subcell at the operating irradiation intensity to avoid the building-up of extra charges and local electric-field that reduce device efficiency. By varying the thicknesses or material compositions of individual photoactive layers, the current of two subcells can be matched.

Fabrication of tandem PSCs usually result in three types of configurations: (1) mechanical stacking which involves preparing different subcells on different substrates followed by adhering them together, (2) monolithic approach of preparing subcells on a single substrate and (3) mixed approach of stacking several monolithic cells together mechanically.[40] Monolithic approach, out of these three configurations, dominates in literatures. Depending on what electrode (anode or cathode) is on the substrate, two basic structures are used commonly: regular and inverted. The next sections therefore revisit these common device geometries and materials at the interlayer in tandem PSCs.

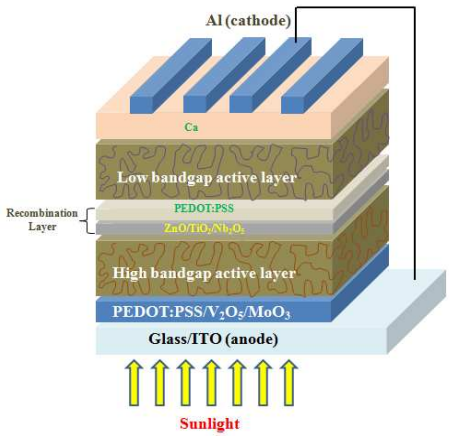

Figure 1 A schematic diagram of tandem PSC in regular architecture

2.1 Regular Structure

A schematic illustrating a regular configuration of tandem PSCs is shown in Figure 1. This structure comprises two polymer/acceptor photoactive layers with different bandgaps for

complementary absorption. The high/wide bandgap photoactive layer is used as the bottom subcell to absorb high energy photons while allowing the low energy photons to pass through. These low energy photons are then absorbed by low bandgap photoactive layer used as the top subcell. One striking feature of regular structure is that the electrode closer to the incident light is the anode which extracts the holes while the cathode which collects electrons acts as a reflective surface for additional light absorption. The recombination layer commonly employed between the two subcells are ZnO [41, 42], TiO_2/TiO_X [43, 44] and Nb_2O_5 [45] as electron transport layer and poly(3,4-ethylenedioxythiophene):poly(styrenesulfonate) (PEDOT:PSS) [23] and MoO_3/MoO_X [44, 46, 47] as hole transport layer. At times thin layers of evaporated metals have also been incorporated into the recombination layers[48-52]. Irrespective of deposition method used, the recombination layer must, in addition, be physically robust not to damage underlying layer(s) and also serve as a protective base for subsequent overlying layer(s).

2.2 Inverted Structure

The inverted architecture of a tandem PSC as shown in Figure 2 comprises wide bandgap photoactive layer as the bottom subcell and low bandgap photoactive layer as top subcell similar to the regular structure. However, the electrodes are reversed with the cathode being closer to the incident light to extract electrons. Inverted device configuration has some benefits over regular ones necessitating its use: (a) incorporation of relatively air-stable high workfunction metals such as silver (Ag) or gold (Au) as anode thereby improving device stability;[53] (b) some polymers in blends with [6,6]-phenyl C_{61} butyric acid methyl ester (PCBM) exhibited vertical phase separation such that rich PCBM phase are closer to the bottom electrode (cathode) resulting in reduced recombination of charge carriers;[54] (c) acidic PEDOT:PSS used at the recombination layer dissolves underneath ZnO layer in regular structure but inverted structure in which acidic PEDOT:PSS has been annealed allows easy and successful ZnO deposition. [55]

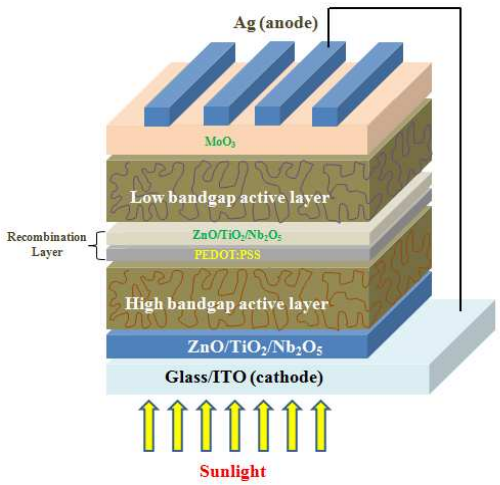

Figure 2 A schematic diagram of tandem PSC in inverted architecture

Inverted structure however has one major downside regarding device processing: the low surface energy of polymer:fullerene blends results in difficulty to subsequently deposit aqueous PEDOT:PSS. This limitation is just for emphasis purpose because various methods employed by researchers to circumvent this problem had been discussed in the later section of this review.

Photovoltaic performance in tandem solar cells can be drastically affected by absorption properties, electrical behavior and layer thickness in the tandem device. These parameters need to be carefully optimized. For example, the overall open-circuit voltage (V_{OC}) of a tandem cell is theoretically equal to the sum of V_{OC} of individual subcells[24]. This may deviate in reality as the tandem V_{OC} can be lower than expected arising from voltage reduction at different layers and particularly at the recombination layer.

The short-circuit current density (J_{SC}) of a tandem cell is typically lower than that of individual subcell. This lower tandem J_{SC} can be attributed either to current mismatch between subcells resulting in imperfect recombination at the recombination layer [56] or lower absorption of the incident light by the back subcell which limits the overall photocurrent. Likewise, light absorption in the back subcells is further reduced in cases where metallic nanoclusters are incorporated into the recombination layer.[57] The V_{OC} on the other hand can be degraded if the thickness of the active layer is large. The increased thickness will increase series resistance of the device which may result in reduced FF as well. The value of FF depends typically on efficient transport and collection of charge carriers in term of series and/or shunt resistances. Therefore, photoactive layer thickness, absorption range, absorption overlap and energy level alignment are important parameters to consider when designing tandem polymer solar devices.

2.3 Double junction cell efficiency estimation

Figure 3 shows the calculated dependence of series-connected double junction polymer photovoltaic performance including V_{oc}, J_{sc}, and cell efficiency (η) on absorption range of front and back subcells. The calculation was performed by assuming: (1) individual subcells optimally absorb the same amount of photon flux and produce identical current density, leading to minimal current loss, (2) individual subcell donor bandgaps (E_g) were obtained from their cutoff absorption wavelengths, (3) V_{oc} of individual subcells was calculated by subtracting E_g from the exciton binding energy (E_b), and (4) FF and EQE were 0.65 and 60%, respectively. Double junction polymer photovoltaic efficiency was finally estimated using the equation [58],

$$\eta_{dj} = \frac{J_{sc-dj} \times V_{oc-dj} \times FF_{dj}}{P_{light}}$$

The J_{sc} of the overall double junction devices increases as the absorption range shifts into the near infrared spectral regions, where higher photon flux is harvested in each subcells. However, the V_{oc} decreases as the donor bandgaps are reduced in individual subcells. The exciton binding energy (E_b) of low bandgap polymers may be similar to these in regular polymers with larger bandgaps. Thus the reduction of polymer bandgaps will lead to a smaller Voc as it is estimated by subtracting E_g from E_b. A compromise between J_{sc} and V_{oc} needs to be obtained in order to

achieve a maximum product ($J_{sc} \times V_{oc}$) at a reasonable FF.

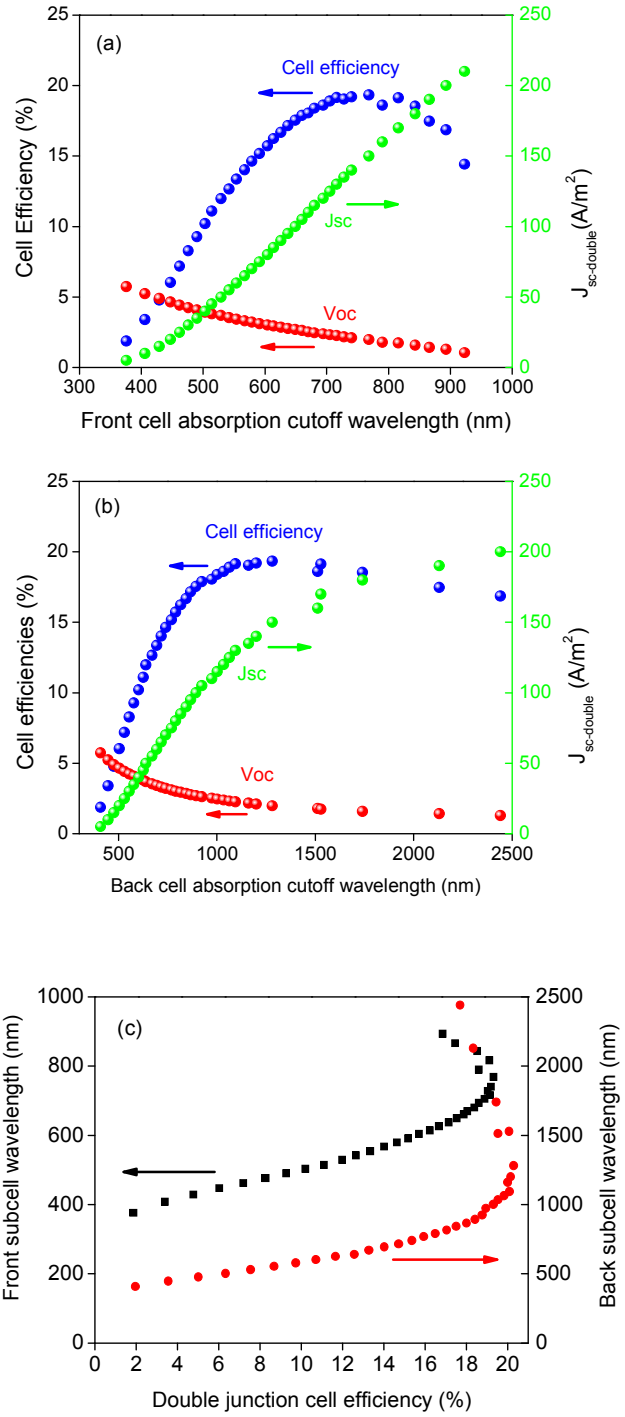

Figure 3 Calculated series-connected double junction polymer photovoltaic performance (e.g. V_{oc}, J_{sc}, and η) dependence on the absorption wavelength of (a) front and (b) back subcell. (c) Relationship between cell efficiency and the combination of subcell absorption spectrum cutoff wavelengths. Reprinted with permission from ref [58].

To achieve the highest possible double junction cell efficiency, both the front and back subcells need to absorb an optimum range of absorption spectra.[58] As shown in Figure 3a and b, the front subcell needs to efficiently absorb up to a wavelength of ~ 775 nm (~ 1.6 eV), while the back subcell should harvest the photons with wavelength up to ~ 1240 nm (~ 1 eV). Also, the HOMO and LUMO energy levels are required to match a specific acceptor with sufficient offset that is no smaller than exciton binding energy for high cell efficiency.

Figure 3c shows a combination of absorption ranges in both front and back subcells in double junction structure for the device efficiency ranging from 2% to ~19.3%. The wavelengths shown in both the left and right y-axis are the cutoff absorption wavelengths. We also noted that the same power conversion efficiency can be achieved from different combinations of subcell absorption spectra. As shown in Table 1, different absorption combinations for the respective front and back subcells can be used to reach cell efficiency from ~ 16.68% to 19.33% and then back to 16.86%. The estimated cell efficiency here is lower than what Minnaert et al. calculated because we used a lower EQE and FF, and a larger D-A LUMO offset.[59, 60]

Table 1 Calculated absorption ranges of front and back subcells and their corresponding double junction cell efficiency.

Front cell absorption range (nm)	Back cell absorption range (nm)	Double junction cell efficiency (%)
626	843	16.68
637	866	17.16
649	893	17.54
660	924	17.89
670	973	18.05
680	1002	18.40
694	1034	18.61
705	1063	18.89
716	1094	19.14
728	1161	19.05
740	1200	19.19
768	1281	19.33
790	1512	18.61
816	1529	19.12
843	1740	18.53
866	2130	17.46
893	2440	16.86

3. Progress in efficiency increase of double junction polymer solar cells

Absorption and thermalization losses in single junction polymer solar cells can be addressed by tandem architecture. A wide and narrow bandgap polymer subcells are usually connected together in different configurations in order to enhance light absorption. Different configurations such as series, parallel, mechanical stacking and folded reflective structures have been reviewed in detail by Siddiki *et al.*[22] Whatever architecture is used, factors such as processability, device performance, and device stability/degradation should be of utmost consideration.

The next section takes a chronological look at representative experimental research in 2010 or later.

3.1 Double junction polymer solar cells

In 2010, Gilot *et al.* optimized tandem PSCs using ZnO nanoparticles and neutral-PEDOT interconnecting layer between PFTBT:$PC_{60}BM$ (1:4 w/w) front and pBBTDPP2:$PC_{60}BM$ (1:2 w/w) back subcell.[41] Figure 4a depicts the device architecture. They used ellipsometer to obtain the refractive indices and extinction coefficients of both polymer:PCBM blend films in order to determine the internal quantum efficiency (IQE). Based on the assumption that highest efficiencies can be achieved in tandem structure when the subcells have identical FF and closely matched current, they matched the J_{SC} and FF of both subcells in the tandem structure with a 180 nm-thick front cell and a 125 nm-thick back cell. Figure 4b shows the experimental J-V behavior for single-junction subcells and tandem cell. The PFTBT:$PC_{60}BM$ front subcell achieved a J_{SC} = 5.5 mA/cm^2, V_{OC} = 0.98 V, FF = 0.52 and PCE = 2.80 %; while the pBBTDPP2:$PC_{60}BM$ back subcell obtained J_{SC} = 6.2 mA/cm^2, V_{OC} = 0.61 V, FF = 0.57 and PCE = 2.16 %. The tandem cell resulted in J_{SC} = 6.0 mA/cm^2, V_{OC} = 1.58 V, FF = 0.52 and PCE = 4.9 %. The result showed that the actual tandem J_{SC} surpassed that of the limiting PFTBT:$PC_{60}BM$ front subcell which had a smaller J_{SC}.

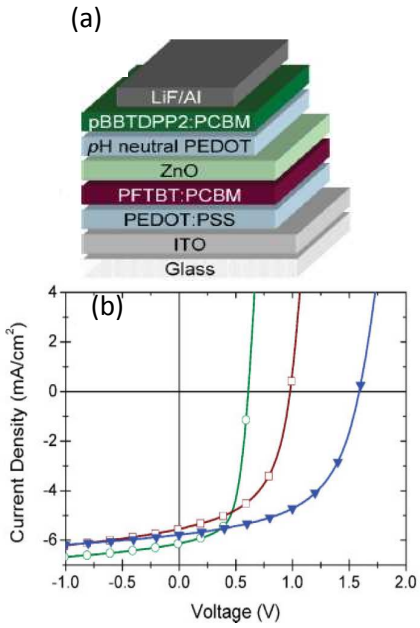

Figure 4 (a) Device architecture and (b) J-V characteristics of PFTBT:PCBM single junction (square), pBBTDPP2:PCBM single junction (circle) and tandem (triangle) solar cells [112]. Note the close current matching from the two subcells. Reprinted with permission from ref [41].

Also in 2010, Sista *et al.* processed P3HT:$PC_{70}BM$ and PSBTBT:$PC_{70}BM$ blends in chloroform for front and back subcells respectively, while the interconnecting layer comprised ultrathin Al layer (0.5 nm)/TiO_2/PEDOT 4083.[61] The ultrathin Al layer was introduced to improve the deposition of TiO_2 as well as ensure that the subcells are electrically connected. Figure 5a depicts device structure, and Figure 5b show the J-V curves of single and tandem cells. The tandem device was then exposed to UV illumination to reduce the energetic barrier and formed an Ohmic contact at TiO_2/PEDOT 4083 interface, leading to a 5.84% tandem efficiency with J_{SC} = 7.44 mA/cm^2, V_{OC} = 1.25 V, and FF = 63.2% (Figure 5b).[61] In 2011, Chou *et al*. employed an inverted architecture incorporating MoO_3 (instead of PEDOT:PSS) interlayer to address the acidic concerns of PEDOT:PSS and significant optical loss (~10%) of PEDOT:PSS.[49] The goal was to provide better stability and optical transparency to the interconnecting layer materials of inverted polymer tandem solar cells. They connected P3HT:$PC_{60}BM$ front and PSBTBT:$PC_{70}BM$ back polymer BHJs using MoO_3/Al/ZnO interconnecting layer. MoO_3 (10 nm) and Al (1nm) were thermally evaporated while ZnO (30 nm) was solution-processed. Transmittance value exceeding 95% in the visible and NIR (near infrared) region was realized for the MoO_3/Al/ZnO interconnecting layer. Figure 6 shows the energy-level diagram of the tandem architecture. The low workfuction cathode contact was ITO/ZnO while the high workfunction anode contact consisted of MoO_3/Al. The interconnecting layer of MoO_3/Al/ZnO facilitated efficient charge recombination of the front and back subcells.

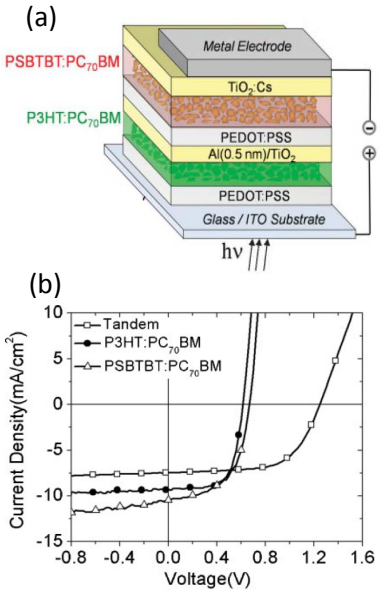

Figure 5 (a) Device architecture and (b) J-V characteristics of P3HT:PC70BM single junction, PSBTBT:PC70BM single junction and tandem solar cells. Reprinted with permission from ref [61].

Single junction reference device of P3HT:$PC_{60}BM$ yielded a J_{SC} = 8.6 mA/cm^2, V_{OC} = 0.58 V, FF = 64% and PCE = 3.2% while that of PSBTBT:$PC_{70}BM$ resulted in a PCE of 3.7 % with J_{SC} = 11.7 mA/cm^2, V_{OC} = 0.64 V, FF = 49%. P3HT:$PC_{60}BM$ was placed as front subcell while PSBTBT:$PC_{70}BM$ was used as back subcell due to the large J_{SC} difference between these two single junction reference devices. Tandem cell subsequently resulted in J_{SC} = 7.8 mA/cm^2, V_{OC} = 1.20 V, FF = 54% and PCE = 5.1%. The V_{OC} of the tandem which was equal to the sum of V_{OC} of component subcells demonstrated effective series-coupling of the two subcells caused by significant vacuum level

shift from the quasi-Fermi level alignment of MoO_3 and ZnO. Later in 2011, in order to further increase tandem device efficiency, Yang *et al*.[62] used a similar device architecture as Sista *et al.,*[61] but they used Ca/Al instead of TiO_2:Cs/Al cathode. In addition, $IC_{60}BA$ was blended with P3HT front subcell to enhance V_{OC} and consequently to increase device PCE. Chlorobenzene was used to process PSBTBT:$PC_{70}BM$ which led to superior J_{SC} (13.7 mA/cm^2) and PCE (4.7%) in single junction cells. Also a physically robust modified PEDOT:PSS (PH500) was developed to ensure that successive layers could be successfully deposited. Figure 7 shows the J-V curves of the P3HT:$IC_{60}BA$ front and PSBTBT:$PC_{70}BM$ back based tandem cells. They achieved 7% tandem PCE with J_{SC} = 7.6 mA/cm^2, V_{OC} = 1.47 V, and FF = 63%.[62]

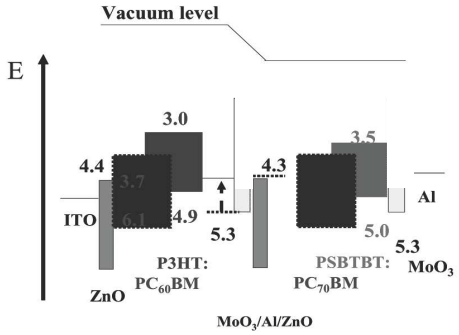

Figure 6 Energy level diagram of P3HT:$PC_{60}BM$ and PSBTBT:$PC_{70}BM$ tandem cell incorporating MoO_3/Al/ZnO interconnecting layer. Reprinted with permission from ref [49].

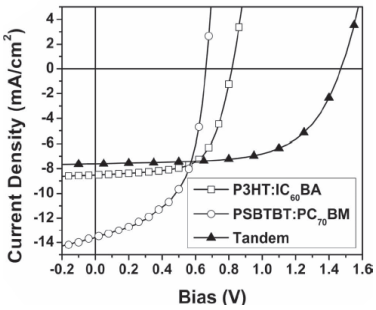

Figure 7 J-V characteristics of P3HT:$IC_{60}BA$ front, PSBTBT:$PC_{70}BM$ back and tandem cells. Reprinted with permission from ref [62].

Most polymer tandem solar cells reported earlier, in a bid to provide all-solution processed fabrication, used either solution-processed ZnO or TiO_X/TiO_2 as one component to ensure efficient recombination at the interconnecting layers in tandem configurations. Noteworthy is the observation that the solution preparation of TiO_X/TiO_2 is relatively complicated, requires longer time (~9 hr) and inert environment.[43] Likewise, ZnO solution processing suffers from potential agglomeration of nanoparticles.[63] However, in 2012, Siddiki *et al*. introduced Nb_2O_5 as a new electron transport layer in the interconnecting layer of a double junction polymer solar cell.[45] They demonstrated the feasible potential of using Nb_2O_5 to provide efficient recombination with pH neutral PEDOT:PSS at the interconnecting layer. The absorption spectra of the MDMO-PPV:PCBM front, back subcells and tandem cell used in their work is illustrated in Figure 8.

Photovoltaic parameters of single-junction front and back subcells, and tandem cells are summarized in Table 2. The realized single junction cell V_{OC}'s are 0.81 V and 0.82 V and the tandem V_{OC} is ~1.3 V which is significantly higher than that of single junction devices but is still less than the expected value for tandem (~1.63 V). For the tandem, J_{SC} was lower and series resistance larger than individual single junction devices. This was attributed to possible current mismatch between the front and back subcells due to additional absorption by the back subcell arising from the reflection of light by aluminum. Also possible interfacial layer barrier might prevent efficient electron-hole recombination at the middle contact resulting in the voltage loss therefore requiring further investigation.

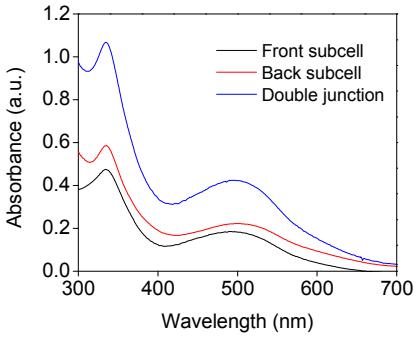

Figure 8 Absorption spectra of MDMO-PPV:PCBM active layers for the front (black), back (red) and tandem (blue) cells. Reprinted with permission from ref [45].

Table 2 Photovoltaic performance parameters of MDMO-PP:PCBM devices for the front, back and tandem cells

Cells	Voc (V)	Jsc (mAcm^{-2})	FF (%)	η	Rse Ωcm^2	Rsh Ωcm^2
Back subcell	0.82	3.7	57.1	1.74	10.2	608.5
Front subcell	0.81	3.46	56.4	1.58	5.9	621.8
Double junction cell (experimental)	1.3	1.5	41.1	0.8	212.6	1489.4
Double junction cell (simulated)	1.58	3.42	33.7	1.82	8.05	615.4

In 2012, Janssen group reported two separate publications on fully solution-processed inverted and regular tandem polymer solar cells. In the first paper, Kouijzer *et al* [55] employed P3HT:$IC_{60}BA$ front and PDPP5T:$PC_{60}BM$ back active layers. Figure 9a shows the inverted device structure. PDPP5T can provide at least 5% efficiency in single junction solar cells and suitable complementary absorption with typical large bandgap polymers in tandem structure. Also PDPP5T:$PC_{60}BM$ (1:2 w/w) blend was processed in a co-solvent of chloroform and *o*-dichlorobenzene (9:1 volume ratio) which exhibited superior device performance. The intermediate recombination layer comprised a continuous 40 nm thick PEDOT:PSS film which was processed by diluting PEDOT:PSS with 25% volume/volume ratio of isopropanol. Subsequently, a 30 nm thick ZnO nanocrystals processed from isopropanol was spin-coated on top of PEDOT:PSS. Because P3HT:ICBA surface is nonpolar and hydrophobic, the authors treated P3HT:ICBA surface with mild N_2 plasma before spin coating acidic PEDOT:PSS. Acidic

PEDOT:PSS solutions can readily dissolve ZnO nanoparticles. To prevent this, the PEDOT:PSS film was first annealed thermally before depositing the ZnO nanoparticles. The inverted tandem cell with 220 nm thick P3HT:ICBA front subcell and 90 nm-thick PDPP5T:PC_{60}BM back subcell demonstrated a J_{SC} = 7.23 mA/cm^2, V_{OC} = 1.35 V, FF = 0.60 and PCE = 5.8 %.[55] This experimentally measured performance of tandem cell closely resembled that of the constructed tandem cell from the individual subcells performance as illustrated in Figure 9c.

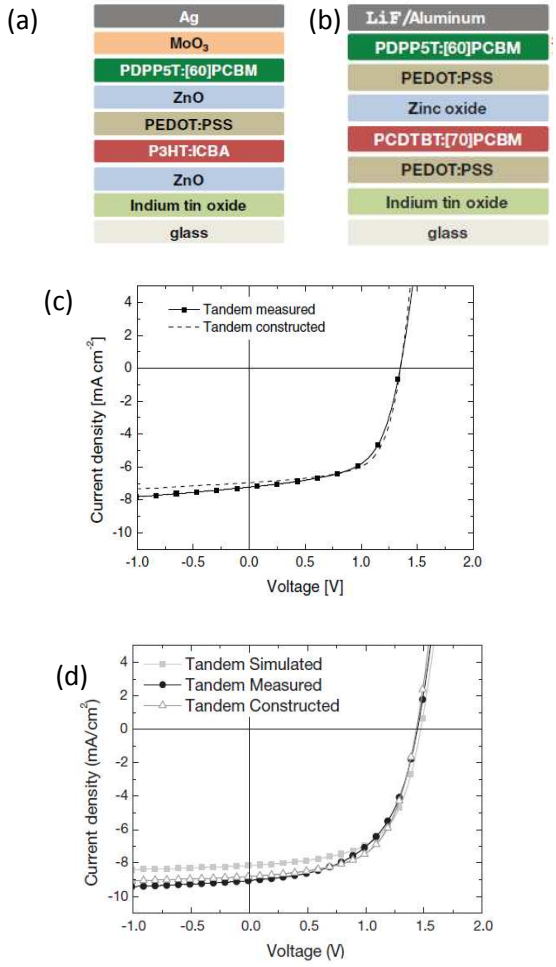

Figure 9 (a) Inverted, (b) regular device architecture; J-V characteristics of measured and constructed (c) inverted P3HT:IC_{60}BA and PDPP5T:PC_{60}BM and (d) regular PCDTBT:PC_{70}BM and PDPP5T:PC_{60}BM tandem polymer solar cells. Reprinted with permission from refs [55, 64].

In their second paper, Gevaerts *et al.* used regular tandem structure with PCDTBT:PC_{70}BM front and PDPP5T:PC_{60}BM back subcells.[64] PCDTBT:PC_{70}BM cell was reported to exhibit a trade-off between the J_{SC} and FF while V_{OC} remained constant enabling the photocurrent to be closely matched with that of PDPP5T:PC_{60}BM cell. Similarly, the intermediate recombination layer comprised a 30 nm thick ZnO nanocrystals processed from isopropanol and a 20 nm thick of neutral pH PEDOT:PSS processed from water. Figure 9b is a schematic view of device architecture. The tandem cell had 170 nm thick PCDTBT:PC_{70}BM active layer in the front subcell and 120 nm thick PDPP5T:PC_{60}BM active layer in the back subcell. The J-V behaviors of the two single junction cells were determined under reduced illumination intensity conditions so that their measured J_{SC} and the J_{SC} obtained from EQE integration were matched. The J-V characteristics of the tandem cell was constructed by adding the two J-V curves of single junctions together following Kirchoff's law and assuming that the recombination layer is loss-free. Figure 9d shows the J-V behavior of the measured tandem cell with J_{SC} = 9.0 mA/cm^2, V_{OC} = 1.44 V, FF = 0.54, and PCE = 7%.[64] This agreed well with the constructed tandem cell obtained by adding the performance of component subcells.

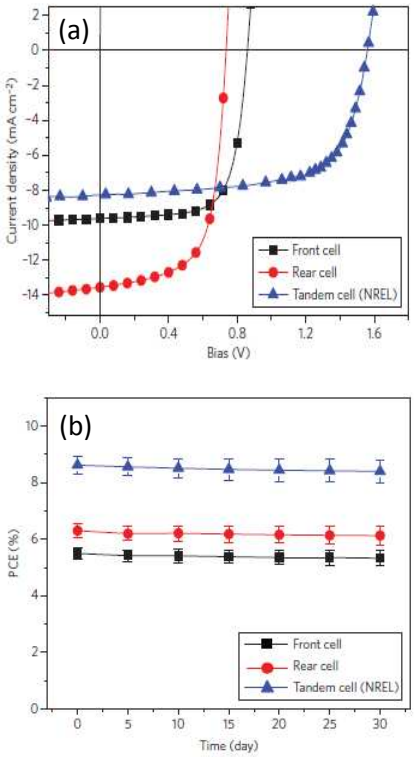

Figure 10 (a) J-V characteristics and (b) stability measurement of P3HT:IC60BA front and PBDTT-DPP:PC70BM rear single and tandem solar cells. Reprinted with permission from ref [65].

Also in 2012, Dou *et al*. in the Yang group fabricated a tandem solar cell using inverted P3HT:IC_{60}BA (high bandgap) and PBDTT-DPP:PC_{70}BM (low bandgap) active layers.[65] The PBDTT-DPP polymer exhibited improved solubility due to its more bulky side-chains and high hole mobility (3.1×10^{-4} cm^{2}V^{-1}s^{-1}) caused by high molecular weight. The high hole mobility enabled a higher J_{SC}. In addition, the deep HOMO level of -5.30 eV helped to achieve a higher V_{OC} in single junction subcells. The PBDTT-DPP:PC_{70}BM (1:2 w/w) blend with an optimal thickness of ~100 nm resulted in a J_{SC} of 13.5 mA/cm^2, V_{OC} of 0.74 V and FF of 65% in single junction cells with a high EQE value (~ 50%) at long wavelengths. In addition, 90% of 300 fabricated devices gave PCEs above 6.0 %. Figure 10a shows the tandem cell performance with a J_{SC} of 8.26 mA/cm^2, V_{OC} of 1.56 V, FF of 66.8%, and a final PCE of 8.62%. In addition to this high efficiency, Figure 10b illustrates that the device performance showed good stability over a period of 30 days after

encapsulation as there was no significant drop in PCE. Further investigations were performed on PBDTT-DPP conjugated polymer by introducing fluorine and selenium into the DPP unit to form PBDTT-FDPP and PBDTT-SeDPP respectively. Efficiency of 8.3% was realized for inverted tandem solar cell incorporating P3HT:ICBA front and PBDTT-FDPP back subcells[66] while that of P3HT:ICBA front and PBDTT-SeDPP back subcells yielded 9.5%.[67]

For the first time, a PEDOT:PSS(PH1000)-polyethylenimine ethoxylated (PEIE) all-organic interconnecting layer was demonstrated by Zhou *et al*.[68] One property of PEIE is its ability to provide workfunction contrast of about 1.3 eV between the two opposite interconnecting interface if thin enough (10 nm). This led to PEIE changing the workfunction of PEDOT:PSS from 4.9 eV to 3.6 eV. P3HT:$IC_{60}BA$ front and PBDTTT-C:$PC_{60}BM$ back subcells connected in an inverted tandem yielded: J_{SC} = 7.7 mA/cm^2, V_{OC} = 1.50 V, FF = 0.72 and PCE = 8.2 %. What was remarkable about this work was that not only was the tandem FF (0.72) much larger than that of individual subcells (0.63 and 0.57), no S-shaped kink was observed in the J-V curve of all the devices. These two factors confirmed an effective carrier selectivity of the recombination layer. Similarly, Kim *et al*. later in 2013 adopted the same interconnection layer combination: PEDOT:PSS and PEIE.[69] The novelty in their work however was a newly synthesized wide bandgap polymer (PTIPSBDT-DFDTQX) as opposed to typically used P3HT. PTIPSBDT-DFDTQX exhibited a deep HOMO level of -5.62 eV and an optical bandgap of 1.85 eV. When PTIPSBDT-DFDTQX:$PC_{70}BM$ (1:2 weight ratio) in chloroform with 3% vol of 1,8-diiodooctane (DIO) was fabricated in regular single junction solar cells comprising ITO/PEDOT:PSS/PTIPSBDT-DFDTQX:$PC_{70}BM$/PFN/Al, a J_{SC} of 10.65 mA/cm^2, V_{OC} of 0.92 V, FF of 62.0%, and a PCE of ~6.1% was achieved. Because of enhanced PCE from 3.5 % in regular to over 5% in inverted single junctions of poly[4,8-bis(5-(2-ethylhexyl)thiophen-2-yl)benzo[1,2-b:4,5b′]-dithiophene-alt-4,7-((2-thylhexyl)thiophen-2-yl)-[1,2,5]-thiadiazolo[3,4-c]pyrid-ine] (PBPT-8) (Eg = 1.56 eV) when blended with $PC_{70}BM$, an inverted tandem of ITO/PEIE/PTIPSBDT-DFDTQX:$PC_{70}BM$/PEDOT:PSS/PEIE/-PBPT-8:$PC_{70}BM$/MoO_3/Ag was constructed. J_{SC} of 7.80 mA/cm^2, V_{OC} of 1.52 V, FF of 0.62 %, and a PCE of ~7.40% was consequently achieved without any kink in J-V behavior.

By aiming to improve the V_{OC} and EQE of low bandgap polymers in single junction cell to complement and enhance the performance of a tandem cell, You *et al*., recently in 2013, reported a certified 10.6% PCE under standard illumination condition (1000 Wm^{-2}, 25 °C).[23] They started from earlier reported low bandgap polymer poly[2,6-(4,4-bis-(2-ethylhexyl)-4H-cyclopenta[2,1-b;3,4-b']-dithiophene)-alt-4,7-(2,1,3-benzothiadiazole)] (PCPDT-BT). Firstly, they introduced two fluorine atoms to act as electron withdrawing unit on benzothiadiazole (BT) unit to form difluorobenzothiadiazole (DFBT) unit with the objective of lowering the HOMO level. Secondly, they inserted an electron-donating oxygen atom to cyclopentadithiophene (CPDT) unit to form dithienopyran (DTP) unit in order to lower the bandgap. The resulting novel polymer poly[2,7-(5,5-bis-(3,7-dimethyloctyl)-5H-dithieno[3,2-b:2',3'-d]pyran)-alt-4,7-(5,6-difluoro-2,1,3-benzothiadiazole)] (PDTP-DFBT) exhibited deep HOMO level of -5.26 eV, high hole mobility of 3.2×10^{-3} cm^{2}V^{-1}s^{-1} using space-charge-limited-current method and a bandgap of 1.38 eV. Inverted single junction devices based on PDTP-DFBT resulted in J_{SC} of 17.8 mA/cm^2, V_{OC} of 0.68 V, FF of 65.0%, and a PCE of 7.9%. This performance in single junction, observable EQE peak which is over 60% (~ 55% on average) and a photoresponse extending up to 900 nm shows a suitable potential for tandem solar cell application. The inverted tandem structure comprises a P3HT:ICBA front subcell and a PDTP-DFBT:$PC_{60}BM$ back subcell with PEDOT:PSS/ZnO interconnecting layer. The cathode and anode consist of ITO/ZnO and MoO_3/Ag respectively. As shown in Figure 11, the tandem J-V behavior certified by National Renewable Energy Laboratory (NREL) resulted in J_{SC} of 10.1 mA/cm^2, V_{OC} of 1.53 V, FF of 68.5%, and and for the first time a double-digit PCE of 10.6% for a polymer tandem solar.

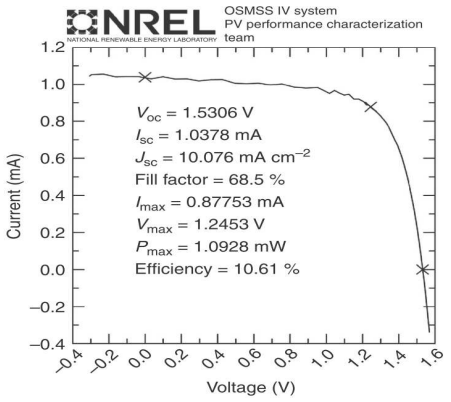

Figure 11 J-V behavior of P3HT:ICBA front and PDTP-DFBT:$PC_{60}BM$ back subcells as measured by NREL. Reprinted with permission from ref.[23]

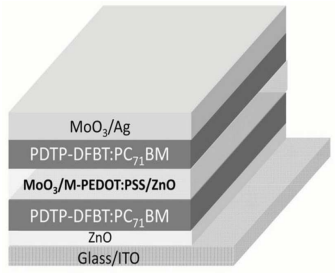

Figure 12 Device structure of inverted tandem solar cell based on two identical PDTP-DFBT:$PC_{70}BM$ photoactive layers. Reprinted with permission from ref [47].

Following the impressive single junction photovoltaic performance of PDTP-DFBT (particularly its high J_{SC}), You *et al*. once again constructed a tandem solar cell with identical subcells of PDTP-DFBT:$PC_{70}BM$ to enhance PCE with the intention of increasing light absorption.[47] Their motivation was a noticeable average light absorption which is still insufficient (less than 60%) in the visible region for the optimized devices. In addition, further increase in the thickness of the active layer degrades PCE arising from charge recombination loss thus justifying their

Table 3: A non-exhaustive list of recent high efficiency progress reported in tandem polymer solar cells.

Year & structure	Electrode	Front subcell active layer	Interconnecting layer	Back subcell active layer	Electrode	J_{SC} (mA/cm^2)	V_{OC} (V)	FF	PCE (%)	Ref.
2010 Regular	ITO+PEDOT:PSS-4083	PF10TBT:$PC_{60}BM$	ZnO+ modified PEDOT:PSS-pH500+Nafion	PF10TBT:$PC_{60}BM$	LiF+Al	3.49 at 0.9mW/cm^2	1.92	0.61	4.5	42, 70
2010 Regular	ITO+PEDOT:PSS-4083	PFTBT:$PC_{60}BM$	ZnO+pH-neutral PEDOT:PSS	PBBTDPP2:$PC_{60}BM$	LiF+Al	6.0	1.58	0.52	4.9	41
2010 Regular	ITO+PEDOT:PSS-4083	P3HT:$PC_{70}BM$	Al+TiO_2+ PEDOT:PSS-4083	PSBTBT:$PC_{70}BM$	TiO_2+Al	7.44	1.25	0.63	5.84	61
2011 Inverted	ITO + ZnO	P3HT:$PC_{60}BM$	MoO_3/Al/ZnO	PSBTBT:$PC_{70}BM$	MoO_3/Al	7.8	1.20	0.54	5.1	49
2011 Regular	ITO+PEDOT:PSS-4083	P3HT:$IC_{60}BA$	Al+TiO_2+ modified PEDOT:PSS-pH500	PSBTBT:$PC_{70}BM$	Ca+Al	7.6	1.47	0.63	7.0	62
2011 Inverted	ITO+Cs:TiO_2	P3HT:$IC_{60}BA$	PEDOT:Au+ Cs:TiO_2	PSBTBT:$PC_{70}BM$	MoO_3 +Al	6.92	1.457	0.619	6.24	71
2012 Regular	ITO+PEDOT:PSS-4083	SDT-BT:$PC_{70}BM$	TiO_x+ PEDOT:PSS-pH~2	P3HT:$PC_{70}BM$	TiO_x+Al	7.2	1.17	0.62	5.2	72
2012 Inverted	ITO + ZnO	P3HT:$IC_{60}BA$	PEDOT:PSS-IPA (3:1)+ZnO	PDPP5T:$PC_{60}BM$	MoO_3 +Ag	7.23	1.35	0.60	5.8	55
2012 Regular	ITO+PEDOT:PSS-4083	PCDTBT:$PC_{70}BM$	ZnO+pH-neutral PEDOT:PSS-H_20(1:1)	PDPP5T:$PC_{60}BM$	LiF+Al	9.0	1.44	0.54	7.0	64
2012 Inverted	ITO + ZnO	P3HT:$IC_{60}BA$	modified PEDOT:PSS-pH500+ZnO	PBDTT-DPP: $PC_{70}BM$	MoO_3 +Ag	8.26	1.56	0.66	8.62	73
2012 Inverted	ITO + ZnO	P3HT:$IC_{60}BA$	PEDOT:PSS + ZnO	PBDTP-DPP: $PC_{70}BM$	MoO_3 +Ag	8.41	1.58	0.64	8.5	66
2012 Inverted	ITO + ZnO	P3HT:$IC_{60}BA$	PEDOT:PSS + ZnO	PBDTT-FDPP: $PC_{70}BM$	MoO_3 +Ag	8.60	1.57	0.61	8.3	66
2012 Inverted	ITO + ZnO	P3HT:$IC_{60}BA$	PEDOT:PSS + ZnO	PBDTT-SeDPP: $PC_{70}BM$	MoO_3 +Ag	9.44	1.52	0.66	9.5	67
2012 Inverted	ITO + ZnO	P3HT:$IC_{60}BA$	PEDOT:PSS-pH1000 + PEIE	PBDTTT-C: $PC_{60}BM$	MoO_3 +Ag	7.7	1.50	0.72	8.2	68
2013 Regular	ITO+PEDOT:PSS-4083	PCDTBT:$PC_{70}BM$	pH-neutral PEDOT:PSS + ZnO	PMDPP3T:$PC_{60}BM$	LiF+Al	9.58	1.49	0.62	8.9	74
2013 Regular	ITO + GO	PSEHTT:$IC_{60}BA$	TiO_x+ GO	PSBTBT:$PC_{60}BM$	ZnO+Al	8.23	1.62	0.63	8.4	75
2013 Inverted	ITO + ZnO	P3HT:$IC_{60}BA$	PEDOT:PSS + ZnO	PDTP-DFBT:$PC_{60}BM$	MoO_3 +Ag	10.1	1.53	0.685	10.6	23
2013 Inverted	ITO + ZnO	PDTP-DFBT:$PC_{70}BM$	MoO_3+ m-PEDOT:PSS + ZnO	PDTP-DFBT:$PC_{70}BM$	MoO_3 +Ag	11.5	1.36	0.65	10.2	47
2013 Inverted	ITO +PEIE	PTIPSBDT -DFDTQX:$PC_{70}BM$	PEDOT:PSS + PEIE	PBPT-8:$PC_{70}BM$	MoO_3 +Ag	7.6	1.51	0.63	7.2	69

rationalization to stack identical subcells. The two subcells were electrically connected by MoO_3/modified-PEDOT:PSS/ZnO interconnecting layer. MoO_3 which has a workfunction of about 5.6 eV was included in the interconnecting layer to facilitate good Ohmic contact with PDTP-DFBT which has a deep HOMO level of ~ 5.3 eV. The maximum absorption of PDTP-DFBT:$PC_{70}BM$ in single junction increased from 70% in the visible to 90% for two PDTP-DFBT:$PC_{70}BM$ in tandem cells. The photovoltaic performance of PDTP-DFBT:$PC_{70}BM$ in inverted single junction (ITO/ZnO/PDTP-DFBT:$PC_{70}BM$/MoO_3/Ag) was further slightly improved compared to earlier report (PCE = 7.9 %) resulting in a J_{SC} of 18.6 mA/cm^2, V_{OC} of 0.69 V, FF of 63.0%, and a PCE of 8.1%. Figure 12 depicts the device structure of the inverted tandem cell with identical subcells based on PDTP-DFBT:$PC_{70}BM$ photoactive layers. In order to allow sufficient absorption and photocurrent to the rear subcell, the thickness of front subcell was kept around 80 nm while that of rear subcell was varied from 80-120 nm. The inverted tandem with 80 nm front and 100 nm rear subcells yielded the highest device performance with J_{SC} of 11.5 mA/cm^2,V_{OC} of 1.36 V, FF of 65%, and a PCE of 10.2%.

Table 3 is a non-exhaustive list of high efficiency tandem polymer solar cells from 2010 to 2013. With this chronicle, a trend towards low cost and fully solution-processed tandem OPVs becomes obvious without compromising achievable device performance. Present electrodes are still 'unavoidably' non-solution processed but anticipation for solution-processed alternatives, another research frontier, is building.

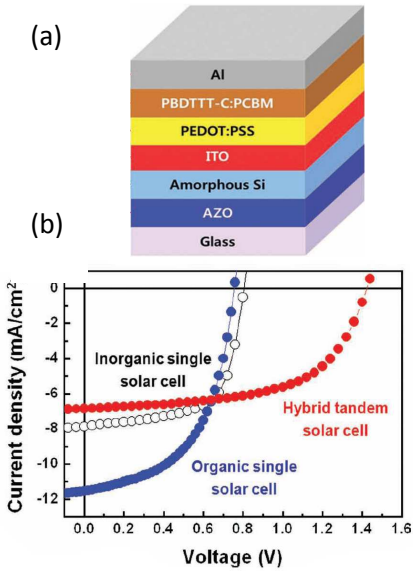

Figure 13 (a) Device structure and (b) J-V characteristics of organic-inorganic single and hybrid-tandem solar cells under illumination of 100 mW/cm^2. Reprinted with permission from ref [76].

3.2 Hybrid double junction solar cells

In 2012, Seo *et al.* developed a hybrid tandem solar cell using organic and inorganic subcells.[76] The front subcell comprised amorphous-silicon (a-Si) (p-type/intrinsic/n-type) deposition using plasma enhanced chemical vapor processing on aluminum-doped zinc oxide (AZO)-coated glass substrate while the back subcell consists a low bandgap poly(4,8-bis-alkyloxybenzo(1,2-b:4,5-b′)dithiophene-2,6-diyl-alt-(alkylthieno(3,4-b)thiophene-2-carboxylate)-2,6-diyl) (PBDTTT-C) blended with PCBM. Figure 13a shows the tandem device structure with magnetron sputtered ITO (50 nm) acting as electron transport layer and spin-coated PEDOT:PSS (70 nm) serving as the hole transport layer. Figure 13b shows the J-V curves of the single junction subcells and tandem solar cells. Using an optimized thickness of 81 nm for the a-Si layer, the tandem device performance exhibited a J_{SC} of 6.84 mA/cm^2, V_{OC} of 1.42 V, FF of 0.58 and a PCE of 5.72 %. The tandem cell using ITO/PEDOT:PSS interface achieved a V_{OC} that was 92 % of the sum of subcell's V_{OC}. This suggested that ITO/PEDOT:PSS intermediate layer successfully connected the two subcells.[76]

4. Issues in double junction polymer solar cells

To achieve a high efficiency tandem polymer solar cell, proper attention and understanding need to be directed to different aspects of tandem device fabrication and measurement. Tandem solar cell material and device engineers should be conversant with experimental issues ranging from (1) selection of complementary absorption photoactive materials and alternative approaches to realize sufficient light absorption by different subcells, (2) demonstration of successful solution-based layer-by-layer deposition, (3) effective current matching in serially connected subcells to maximize short-circuit current density (J_{sc}), (4) effective carrier extraction and carrier collection at the electrodes as well as balanced carrier recombination at the interconnecting layers, (5) accurate or reliable measurement of external quantum efficiencies (EQEs) of individual subcells in tandem PSCs to further probe into the performance-limiting subcells of the tandem devices. Detailed and commendable reviews had been presented on EQE measurement of tandem solar cell by various groups[77, 78] and as a result they will not be discussed in this review. Interestingly, a number of research works on tandem based on optical and/or electrical simulations had been reported that not only verified experimental results [79-83] but also showed the potential of tandem PSCs. [59, 84] Practical demonstrations still have room for further performance improvement. Hence, this section extensively highlights common experimental material and design issues that limit the development of high efficiency solution-processed tandem PSCs. Most importantly, we also pointed out various approaches presently taken to surmount these issues in order to achieve mechanically robust, optically effective and electrically efficient tandem solar devices.

4.1 Mechanical property

Since all the subcells are deposited by solution-based processing and the active layer materials are typically soluble in common solvents, the deposition of top subcells can destroy the underneath subcells if not protected carefully. The intermediate layer in tandem polymer solar cells should be physically robust

enough to protect the top subcell while not destroying the underlying subcell. Various methods have been adopted by researchers to achieve mechanically stable intermediate layers.

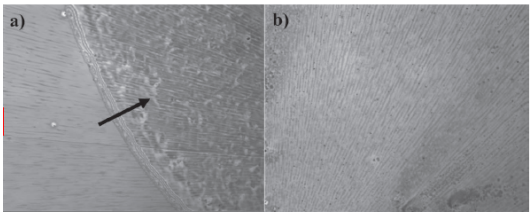

Figure 14 Optical microscope images of (a) traditional PEDOT4083, (b) m-PEDOT films deposited on P3HT:PC70BM layer followed by CB rinsing. Note the arrow in (a) depicts washing off after CB rinsing but unaffected in (b). Reprinted with permission from ref [62].

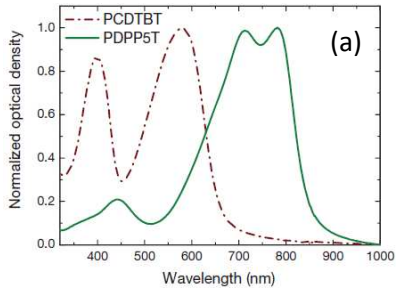

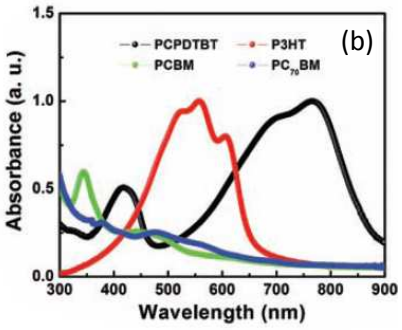

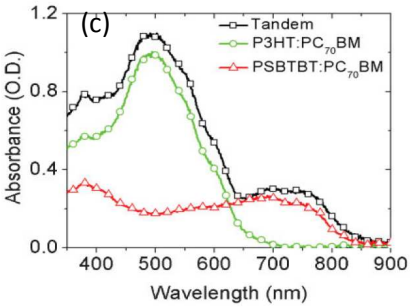

Figure 15 Absorption spectra illustrating complementary absorption of active layers in different tandem architectures (a) PCDTBT and PDPP5T; (b) P3HT and PCPDTBT and (c) P3HT and PSBTBT. Reprinted with permission from refs [43, 61, 64].

Sista *et al.* [61] modified P3HT:$PC_{70}BM$ surface by thermal evaporation of 0.5 nm ultrathin Al to provide wettability and improve the dense packing of subsequently deposited TiO_2 nanocrystalline sol-gel film in order to increase the mechanical robustness. Yang *et al* [62] modified commercial PEDOT:PSS-PH500 with sodium polystyrene sulfonate (SPS) in different ratios to increase mechanical robustness. This PEDOT:PSS was then called modified PEDOT (m-PEDOT). They also added 5% dimethylformamide (DMF) to enhance the conductivity of this m-PEDOT. They tested and compared the mechanical robustness by rinsing the m-PEDOT and traditional PEDOT 4083 surfaces with chlorobenzene (CB). Figure 14 shows the comparison of optical microscope images from (a) traditional PEDOT 4083 and (b) m-PEDOT to illustrate the mechanical robustness. Figure 14a depicts some white regions, showing that PEDOT4083 was not strong enough to protect the underlying P3HT:$PC_{70}BM$ layer which was washed away with CB rinse. This result demonstrated that m-PEDOT is more mechanically robust than the traditional PEDOT 4083. In addition, PEDOT 4083 devices exhibited frequent device shorting after CB rinsing treatment.

A special kind of PEDOT:PSS (Clevios F CPP105D) that was suitable for plastic substrate coatings was diluted with isopropanol and then successfully deposited on hydrophobic P3HT:ICBA surface without poor film formation by Kouijzer *et al.*[55] In addition, they also used isopropanol as solvent to prepare ZnO because the UV-Vis measurement showed that isopropanol did not remove the previously deposited PEDOT:PSS layer. Other researchers have modified pH neutral PEDOT:PSS with either water [63] or mixed water and isopropanol [64] to improve wetting and robustness of PEDOT:PSS on ZnO nanoparticles.

4.2 Optical property

In order to take advantage of wider solar spectra, proper control of light absorption in the photoactive layers of tandem polymer solar cells has been investigated to improve cell performance. In a tandem solar cell, back (rear) subcell harvests the unabsorbed light from front subcell by using complementary absorbing polymers (i.e. high and low bandgap polymers) in blend with suitable fullerene derivatives. In addition, metal nanoclusters were introduced into the intermediate layers to induce plasmon-enhanced light absorption of the back subcells.[71] This section takes a closer look at how these research approaches have increased the efficiencies of tandem polymer solar cells.

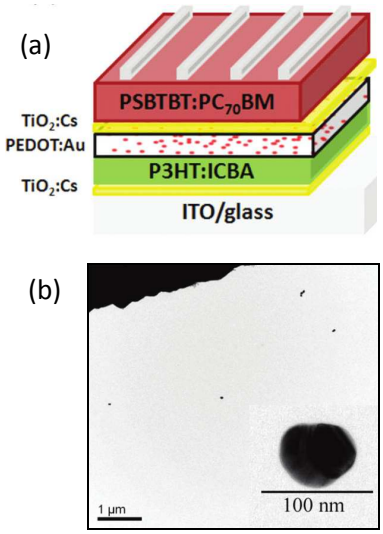

Figure 16 (a) Device structure of plasmonic tandem PSC, (b) TEM images of an Au NP. Reprinted with permission from ref [71].

4.2.1 Use complementary absorption polymers

Complementary absorption spectrum between the front and back subcells is one of the most important parameters to achieve high efficiencies in organic tandem devices. A common approach to tune the bandgaps and absorption spectra of conjugated polymers is to use alternate electron-rich (donor) and electron-deficient (acceptor) moieties on the polymer backbone in a push-pull strategy.[43, 55, 61, 64] By alternating the electron-rich and electron-deficient units, internal charge transfer process is enhanced along the conjugation chain resulting in increased effective resonance length of π-electrons. This strategy has been widely used particularly in the design of polymers with small bandgaps. In addition, certain acceptors such as fullerene derivatives can enhance light absorption in tandem solar cells and compensate for unavoidable absorption gaps in conjugated donor polymers.[37, 85, 86] Figure 15a shows the complementary absorption spectra of PCDTBT and PDPP5T conjugated donor polymers reported by Gevaerts *et al.* in their tandem solar cells[64]. PCDTBT with an optical bandgap of ~1.88 eV mainly absorbed light within 325 – 660 nm, while PDPP5T exhibited an optical bandgap of ~1.46 eV and harvested 650 – 875 nm of light; some spectral overlap could be observed between PCDTBT and PDPP5T at about 600 nm. It is important to observe absorption gap between 420 nm and 550 nm in PCDTBT; the authors carefully selected $PC_{70}BM$ which has characteristically stronger absorption in 450-550 nm wavelength range to compensate for this absorption gap. Tandem solar cells using PCDTBT:$PC_{70}BM$ front and PDPP5T:$PC_{60}BM$ back subcells, as a result, achieved an efficiency of 7%. Figure 15b shows the complementary absorption spectra of P3HT and PCPDTBT donor polymers. P3HT has good interchain packing and hole mobility (0.1 cm^2/V-s).[87] P3HT with an optical bandgap of ~1.9 eV showed an absorption in the spectral range of 350-650 nm, while 1.4 eV bandgap PCPDTBT absorbs within 550 – 900 nm. 6.5% efficiency was realized in a P3HT:$PC_{70}BM$ and PCPDTBT:PCBM tandem polymer solar cell. Figure 15c illustrates the absorption spectra of P3HT:$PC_{70}BM$ front and PSBTBT:$PC_{70}BM$ back subcells in the tandem structure reported by of Sista *et al.*[61] Due to the significant absorption overlap of the two subcells between 350 nm to 650 nm, the light intensity absorbed by rear subcell (PSBTBT:$PC_{70}BM$) was reduced by ~ 40% after passing through the front subcell (P3HT:$PC_{70}BM$. Sista *et al.* however observed that when incident light intensity of 1 sun was reduced by half in single junction PSBTBT:$PC_{70}BM$ device, the shunt resistance and ultimately PCE improved by 10% because of significant reduction in non-germinate recombination. This explanation suggested the reason why PSBTBT:$PC_{70}BM$ could still function as an effective rear subcell and a final tandem efficiency of 5.84% was achieved.[61] These diverse issues should be carefully considered when designing and fabricating a tandem polymer solar cell to maximize the optical property of both subcells in the tandem.

4.2.2 Apply plasmonic effect to enhance light absorption of both front and back subcells

The subcell thickness cannot be unlimitedly increased to absorb more sunlight due to inefficient charge transport in organic materials. Recently Yang *et al.* reported that blending Au nanoparticles (NPs) into the intermediate layers that connect two subcells can induce plasmonic effect to enhance light absorption of both subcells.[71] The electromagnetic (EM) field of incident light undergoes resonant interaction with the surface electron density around metallic nanoclusters resulting in localized EM enhancement, which can improve light harvesting through selective light absorption in the wavelength region of interest [88]. The shape, size and dielectric constant of the metallic NPs also affect the resonance peak.[89] In small molecule tandem solar cells, silver nanoclusters were inserted into the intermediate layers to serve as recombination centers for charges from adjacent subcells and induce strong near-field to increase active layer light absorption.[71, 90] Plasmonic effect in single BHJ polymer solar cells has been demonstrated with noticeable PCE enhancement spurring recent utilization of this concept in tandem PSC architecture.[89, 91, 92] The interconnecting layer selected by Yang *et al.* [71] in their tandem cell comprised TiO_2:Cs n-type buffer layer and 70-80 nm-sized Au metal nanoclusters blended into PEDOT:PSS p-type interconnecting layer to enhance absorption of both subcells. Figure 16a shows a schematic of tandem polymer solar cell with the plasmonic Au nanoparticles embedded in the PEDOT:PSS layer at a thickness of 70-80 nm. Figure 16b shows transmission electron microscopy (TEM) image of an Au nanoparticle with a size of 70-80 nm. 10 nm thick TiO_2:Cs was used as electron transport layer. Since the Au nanoparticle was similar to PEDOT:PSS thickness and TiO_2:Cs was very thin, the authors concluded that the gaps between the Au NPs and front or back subcells were negligible.[71] This implies that both the active layers in the front and back subcells are within the local near-field region of Au NPs; thus enhanced light absorption in both front and back subcells by the near-field of surface plasmon.[71]

Figure 17a depicts absorption spectra of tandem solar cells with and without Au NPs. It shows that incorporation of Au NPs into the PEDOT layer increased light absorption in the regions of 450-650 nm and 750-850 nm. Enhancement in the 450-650 nm region was attributed to the plasmon resonance of Au NPs, which is consistent with spectrum in the inset of Figure 17a. However, the 750-850 nm region was far from the Au NP plasmon resonance spectrum, which was then explained by extended plasmonic resonance via Au NP aggregation in the PEDOT layer.[71] Figure 17b and c show the J-V curves and external quantum efficiency (EQE) of tandem solar cells with and without Au NPs under AM1.5G 100mW/cm^2 illumination. After introducing Au NPs, tandem solar cells exhibited a significantly increased J_{SC}, slightly enhanced FF and unchanged V_{OC}. The J_{SC} increased from 6.06 to 6.92 mA/cm^2, leading to a PCE improvement from 5.22 to 6.24%. The EQE was also increased from 32.6 to 41.7% for front subcell and from 48.1 to 53.1% for back subcell. The J_{SC} and EQE increase was attributed to the increased light absorption in both front and back subcells caused by the near-field of surface plasmon from the incorporated Au NPs. The slightly decreased EQE in 400-600 nm indicated that incorporation of Au NPs has absorbed more light in the front cell, leading to less light for back cell.

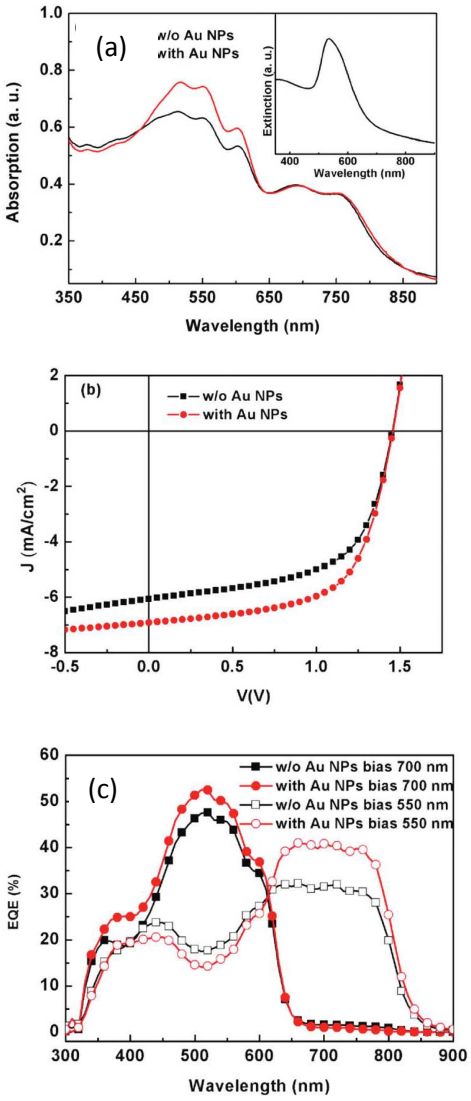

Figure 17 (a) absorption spectra, (b) J-V curves, and (c) EQE of tandem solar cells with and without Au NPs. The inset in (a) shows the extinction spectrum of Au NP solution. Reprinted with permission from ref [71].

Table 4: Performance comparison of tandem and single junction cell with and without Au NPs [71].

Device	V_{OC}(V)	J_{SC} mA/cm^2)	FF (%)	PCE (%)
w/o Au (tandem)	1.455	6.06	59.22	5.22
With Au (tandem)	1.457	6.92	61.91	6.24

Since the ideal light harvesting in the active layers from the subcells has complementary absorption spectral range without overlap, the transmission loss caused by the active layers will be insignificant. Also, most of interfacial layers including electron transport, hole transport and interconnecting layers are made of large bandgap polymers and are transparent, which will not cause much loss in the transmission. However, the reflections at the various interfaces in double junction multilayered device architecture may cause some transmittance loss, which can be estimated by optical simulation at those interfaces. Based on such simulation results, optical interfacial layer materials and thickness of active layers can be found out. In addition, previous modelling of optical field distribution in the different device structures suggested that higher current density from inverted structures was caused by enhanced absorption of incident light in the active layer.[93] The inverted structures have less parasitic absorption in the PEDOT:PSS and the Ca layer which are used in normal structures. [93]

4.3 Electrical property

Series-connected subcells in tandem structure should support Kirchoff's law: tandem V_{OC} should be approximately the sum of V_{OC} of component subcells. Likewise, the electrical characteristics of component cells should reflect in the constructed tandem. One of the common problems in series-connected tandem is resistive or potential loss at the interlayer connecting the two subcells. This section gives an overview of observed limitations and approaches employed to mitigate them.

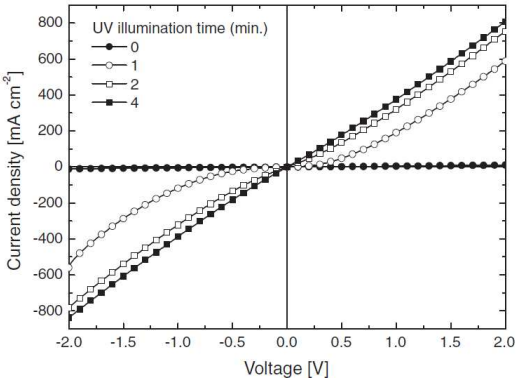

Figure 18 J-V curves of a simplified ITO/PEDOT:PSS/ZnO/Ag device at different time of UV illumination on the interconnecting contact. Reprinted with permission from ref [55].

4.3.1 UV illumination or light soaking

To achieve efficient electrical connection between subcells, the interconnecting layer must provide efficient recombination site of electrons and holes without charge carrier accumulation. The interconnecting layer should function electrically such that Ohmic contact is formed between the subcells. One way to achieve this is through sufficient doping of electron transport layer (e.g. ZnO, TiO_2, Nb_2O_5, etc) and hole transport layer (e.g. PEDOT).[63] PEDOT is typically doped with PSS, while ZnO, TiO_2, Nb_2O_5 can be doped by UV irradiation[63] or light soaking.[94]

Kouijzer *et al.* [55] prepared a simplified ITO/PEDOT:PSS/ZnO/Ag device and then tested PEDOT:PSS/ZnO intermediate contact performance with and without UV illumination. Figure 18 shows J-V curves of a simplified ITO/PEDOT:PSS/ZnO/Ag device at different time (0, 1, 2 and 4 min) of UV illumination on the interconnecting contact. It can be seen that better Ohmic contact was formed as UV illumination time increased from 0 to 4 min. Doping by UV illumination was found to saturate at 4 min for this specific batch of ZnO layer, but varied for other batches. This indicated that the ZnO layer was doped by the photoinduced carriers generated by UV illumination. It has also been observed that after prolonged storage of UV-illuminated single or tandem devices in the dark, the high resistive state at the interconnecting layer is restored.

Therefore, repeated UV illumination is required to remove the S-shape J-V curves.[94, 95] Other researchers had also demonstrated that UV light treatment on ZnO/PEDOT:PSS interlayer can improve device performance by forming Ohmic contact at the interconnecting layer.[63]

Similarly, Sista *et al*. employed a 400 nm cutoff filter on the solar simulator to add or remove UV illumination.[61] When the UV part of the solar spectrum was blocked with this filter, an 'S-shaped' curve around the V_{OC} was observed both in single and tandem devices. The single junction device ITO/PEDOT4083/P3HT:$PC_{70}BM$/UT-Al/TiO_2/PEDOT:PSS/Al used ultrathin(UT)-Al/TiO_2/PEDOT:PSS interface. The tandem cell is ITO/PEDOT:PSS/P3HT:$PC_{70}BM$/UT-Al/TiO_2/PEDOT:PSS/PSBTBT:$PC_{70}BM$/TiO_2:Cs/Al, in which UT-Al/TiO_2/PEDOT:PSS was used as interconnecting layer. This S-shape was reported to be caused by an interfacial barrier for charge transport at the interconnecting layer.[96] Sista *et al*. applied UV exposure on both single and tandem cells by removing the 400 nm cutoff filter.[61] Figure 19a shows J–V curves of single and tandem cells before and after removing the 400 nm cutoff filter. It was found that 'S-shaped' curves vanished in both single and tandem solar cells after removing the filter. Figure 19b shows the energy level diagram of tandem cells with TiO_2/PEDOT4083 as an intermediate layer, which was proposed by Sista *et al.* TiO_2 exhibited a quasi-Fermi level that is close to PCBM LUMO in the front subcell, while the heavily doped PEDOT:PSS had a high workfunction that was close to the donor polymer HOMO in the back subcell. As shown in Figure 19b, this formed an interfacial triangular barrier for electrons from the front subcell to tunnel or recombine with holes from the back subcell, leading to a S-shape in J-V curves.[61] When carrier concentration is low in TiO_2, the width of triangular barrier is large, which makes the tunneling or recombination difficult. However, the carrier concentration can be significantly increased by the photogenerated carriers from UV illumination. The higher carrier concentration will reduce the barrier width and make it thin enough for tunneling or recombination to occur. This is the reason that UV illumination can result in a Schottky-to-Ohmic transition to remove the S-shape and increase tandem solar cell performance. Similar scenario of the need to photodope TiO_2 [97] or TiOx [72] and consequently enhance its carrier concentration to realize higher efficiency in solution-processed tandem PSC had also been observed and reported.

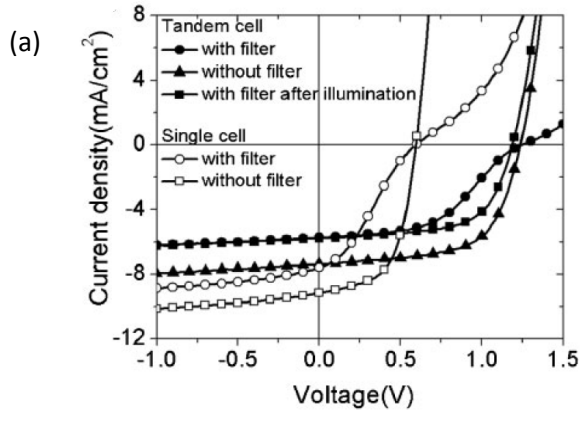

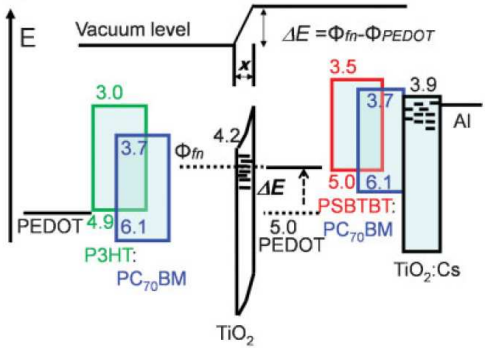

Figure 19 (a) J–V curves of single cells and tandem cells with and without a 400 nm cutoff filter, and (b) proposed energy level diagram of tandem cells with TiO_2/PEDOT4083 as an intermediate layer by Sista *et al.* Reproduced with permission from ref [61].

4.3.2 Energy band alignment of interconnecting layers with active layers

It is important that the energy bands of interconnecting layers properly align with that of respective active layers in tandem PSCs. This implies that in tandem PSCs, Ohmic contacts need to be formed between the HOMO energy level of donor polymer and effective energy band of adjacent hole-collecting interconnecting layer as well as between the LUMO energy level of acceptor polymer and effective energy band of electron-collecting interconnecting layer. This Ohmic contact formation is necessary in order for the tandem device performance not to suffer from substantial energy or V_{oc} loss. In addition, the two (or sometimes more) materials selected as interconnecting layers in tandem PSCs must be solution-processed in orthogonal solvents in order not to dissolve or damage each other. Likewise, their wetting behavior should be carefully observed. Based on these considerations, numerous published reports on solution-processed tandem polymer solar cells adopted a number of n-type interconnecting layers such as ZnO,[63, 98] TiOx,[72, 80-82] Nb_2O_5,[58, 99] and PEIE [68, 69]; as-received or modified aqueous (i.e. water-based) PEDOT:PSS,[72, 100] MoO_3 [101, 102] or graphene-oxide [75] are commonly used as the p-type interconnecting layer. It is noteworthy to mention that commercial PEDOT:PSS is the dominantly employed p-type interconnecting layer (see Table 3). This widespread use of PEDOT:PSS is possibly due to: (1) PEDOT:PSS being water-based provides sufficient robustness that prevents its dissolution by n-type interconnecting layer typical processed in organic solvents and (2) PEDOT:PSS (~5.1-5.2 eV) forms suitable band-alignment with most donor polymers employed in tandem PSCs. As the current trend towards synthesis of conjugated donor polymers with deep HOMO level (< -5.2 eV) becomes inevitable to realize higher V_{oc}, it becomes even more important for researchers to begin critical search for solution-processed p-type materials that can provide energy-level matching with deeper HOMO level polymers. This necessity for energy-level matching was emphasized by Moet *et al*. in 2010 during their fabrication of organic tandem solar cells using neutral PEDOT-ZnO middle electrode.[42] The pH value of highly conductive PEDOT:PSS (Clevios PH500) was modified by 3.0 vol % of 2-dimethylaminoethanol (DMAE, Aldrich):water (1:8 dilution). From UV-Vis absorption spectroscopy, acidic PEDOT:PSS with a pH less than 3 was found to dissolve ZnO

layers; also poor quality of wetting or film formation was noticed. A PEDOT:PSS with pH ≥ 3 was therefore recommended to be compatible with ZnO layers and a pH of 3.4 called M-PH500 was eventually used in their solar cell devices. To demonstrate their idea of energy band alignment requirement, they compared the performance of two double junction solar cells having identical active layers as front and back subcells. One incorporated P3HT which had an ionization potential of ~4.8 eV and the other incorporated poly[9,9-didecanefluorene-alt-(bis-thienylene)-benzothiadiazole] (PF10TBT) that had higher ionization potential (~5.4 eV). A reduced V_{OC} was expected if a non-Ohmic contact or energy barrier existed between the HOMO of these polymers and neutral PEDOT. Single junction devices with ITO/neutral-PEDOT:PSS/P3HT:PCBM/LiF/Al resulted in a V_{OC} of 0.55 V while a V_{OC} of 1.10 V which was the sum of those of single junctions (0.55 V + 0.55 V) was realized in double junction solar cells connected by neutral-PEDOT:PSS-ZnO middle layer. This indicated that interconnecting layers did not introduce any energy barrier or limitation to device performance of donor polymers with ionization potential of 4.8-4.9 eV such as P3HT. On the other hand, ITO/neutral-PEDOT:PSS/PF10TBT:PCBM/LiF/Al single junction solar cells yielded ~1.0 V but a paltry V_{OC} of 1.5 V could only be achieved in double junction devices as opposed to expected 2.0 V. The origin of this problem was exposed by Kelvin probe (KP) measurement as shown in Figure 20. As the pH of PEDOT:PSS (PH500) was increased from 1.9 (unmodified) to 8, the workfunction strongly decreased. Likewise, V_{OC} of PF10TBT:PCBM (1:4) single junction decreased by ~0.5 eV at pH 3.4 highlighting the reason for the V_{OC} loss encountered in the double junction solar cells. Nafion-like compounds had been previously calculated to usually exhibit higher ionization potential than polystyrene sulfonic acids (PSS). [103, 104] A thin layer of Nafion perfluorinated resin solution after high dilution in ethanol was thus spin-coated on top of M-PH500 to recover the workfunction and suitably align the energy band between M-PH500 and PF10TB. Consequently, a V_{OC} of 1.92 V and efficiency of 4.5 % was finally achieved for the double junction solar cell. This additional step of device processing (i.e. Nafion inclusion) could have been avoided if suitable p-type material was available.

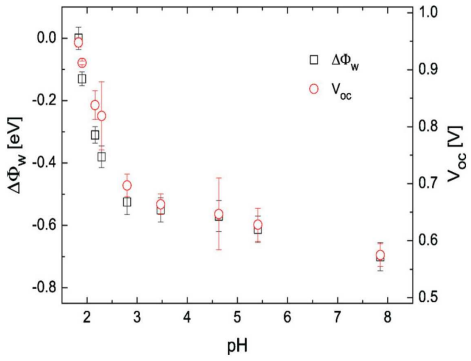

Figure 20 Effect of pH-modified PEDOT:PSS (PH500) on the work function of ITO/45 nm thick M-PH500 layers:(squares) and V_{OC} of PF10TBT:PCBM single junction solar cells (circles). Reproduced with permission from ref [42]

Recently, You *et al*. in 2013 reiterated the critical role of the interconnecting layer in series-connected tandem polymer solar cells.[47] The reason for their emphasis is that modified PEDOT:PSS (called M-PEDOT:PSS) which was previously and consistently demonstrated as an effective interconnecting layer combination with ZnO in inverted tandem solar cells [23, 62, 65] suddenly and unfortunately could not effectively function when PDTP-DFBT:$PC_{70}BM$ was employed as the active layer. One of the possible causes was the same as what Moet *et al*. [42] observed: PDTP-DFBT exhibited deep HOMO energy level (-5.3 eV). From ultraviolet photoelectron spectroscopy (UPS) results shown in Figure 21a, the workfunction of conventional PEDOT:PSS, after being modified by additives, decreased from 5.3 eV to 5.0 eV which was much lower than that of PDTP-DFBT (5.3 eV). Thermally evaporated MoO_3 however with a workfunction of 5.6 eV or even higher [105, 106] provided good Ohmic contact with PDTP-DFBT; this is also illustrated in the energy band diagram of Figure 21b. As shown in Figure 21c, inverted single junction solar cells using M-PEDOT:PSS and MoO_3 therefore resulted in J_{SC} of 17.0 mA/cm^2, V_{OC} of 0.68 V, FF of 0.55, PCE of 6.4% and J_{SC} of 18.6 mA/cm^2, V_{OC} of 0.69 V, FF of 0.63, PCE of 8.1% respectively. Much of the device performance difference was in the J_{SC} and FF in this case. In order to achieve high tandem efficiency in identical PDTP-DFBT:$PC_{70}BM$ front and PDTP-DFBT:$PC_{70}BM$ back subcells, a MoO_3 (15 nm)/M-PEDOT:PSS/ZnO interconnecting layer was employed resulting in 10.2% efficiency. Although this tandem efficiency was high enough, note that MoO_3 was thermally evaporated while M-PEDOT:PSS and ZnO were processed from solution. It is therefore necessary for material scientists in the future to begin search for complementary p-type interconnecting materials that (1) is solution-processable and (2) has deeper energy band level than PEDOT:PSS to reduce cost, fabrication complexity and processing time of tandem PSCs.

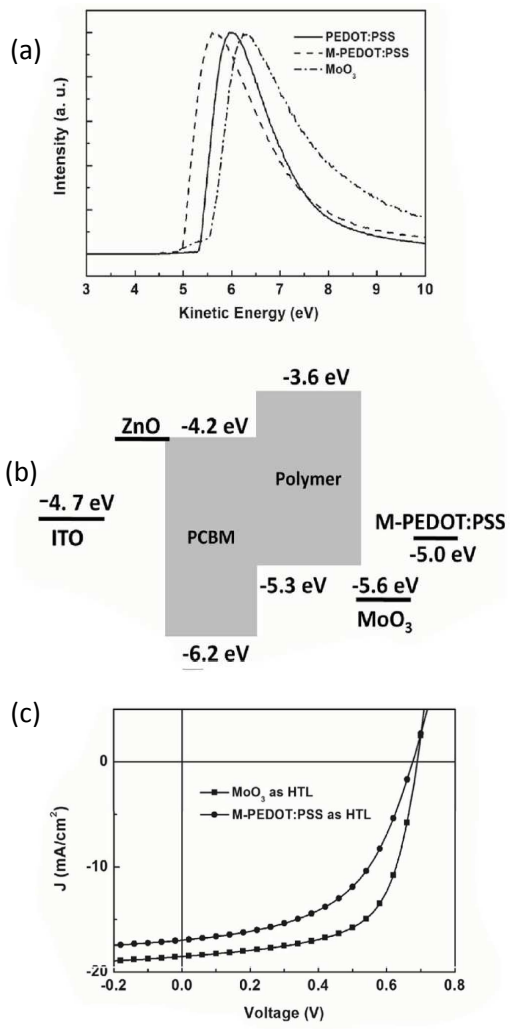

Figure 21 (a) ultraviolet photoelectron spectroscopy of PEDOT:PSS, M-PEDOT:PSS and MoO_3; (b) energy band diagram of inverted single junction cell illustrating the need for good band alignment at the polymer:HTL contact; (c) J-V curves of inverted single junction cell based on 100 nm thick PDTP-DFBT:$PC_{70}BM$ active layer with MoO_3 and M-PEDOT:PSS hole transport layers (HTLs). Reproduced with permission from ref [47]

5. Conclusion and outlook

As central to the operation of double junction polymer solar cells, the photoactive layers should provide complementary absorption by absorbing different regions of solar spectra with high optical densities enabling maximum use of photon energies. Successful design and synthesis of low bandgap polymers has resulted in relatively large number of efficient single-junction devices that have been integrated into highly efficient tandem geometry. Presently, there is no viable substitution for P3HT which is still the dominant wide bandgap polymer of choice. The road towards 15 % efficiency in tandem polymer solar cell requires further exploration of this research area by chemists or material scientists. The interconnecting-layer design is also critical to ensure that subcells are successfully connected by providing efficient recombination of opposite charge carriers. Ohmic contact between these layers and photoactive layers is necessary for high efficiency; otherwise the total V_{OC} lesser than the sum of individual subcell V_{OC} is typically observed. In addition, inexpensive solution-processing of OPVs has been made possible for successful and robust deposition of each layer and subsequent ones. In spite of these requirements, this review, by discussing various technological, device and processing issues, shows that some of these constraints have been overcome. Despite being solved, it is possible that in the future, some of these constraints will resurface. As a result, various approaches leading to this success were carefully highlighted resulting in some high efficiency tandem polymer solar cells with PCEs between 8-11% that had been demonstrated in recent years. This accelerated development and efficiency progression in tandem polymer solar cells will further confirm the prospect of OPV technology in coming years. New materials, robust processing, novel device design and device modelling have supported understanding of the operation and fabrication of tandem polymer cells.

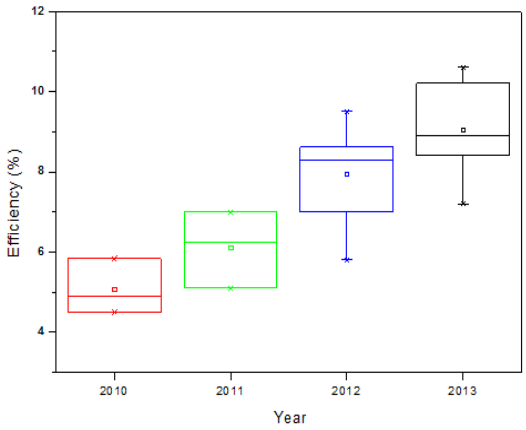

Figure 22 Power conversion efficiency evoluation of double junction polymer solar cells reported from 2010 to 2013.

Figure 22 is a non-exhaustive depiction of recent power conversion efficiency evolution made in solution-processed tandem polymer solar cells. The highest reported efficiency increased from ~ 6% in 2010 to ~ 10.6% in 2013. It is important to mention that 12% record efficiency has been reported by Heliatek GmbH for vacuum-processed small molecule tandem solar cells. This trend in the increase of tandem OSC efficiency is remarkable and efforts are being geared towards 15% efficiency by 2015. This milestone is possible judging from the fact that there is still a lot of room that can be improved in tandem polymer solar cells: (1) absorption spectra in the near infrared region are not broad enough; (2) external quantum efficiencies are still not high in a broad spectral regions; (3) light trapping/absorption techniques such as incorporating antireflection coating, optical spacer and plasmonic effect have not been fully investigated. The efficiency projection and possible research breakthroughs further highlight a promising future for OPV as a commercially viable venture in cost effective photovoltaic techniques.

Acknowledgements

We acknowledge the financial support from US NSF CAREER award (ECCS-0950731), NASA EPSCoR (NNX13AD31A),

National Science Foundation/EPSCoR Grant No. 0903804, NSF IGERT program, and South Dakota Board of Regent CRGP.

References

1. P. B. Weisz, *Physics Today*, 2004, **57**, 47.
2. C. Rühl, BP statistical review of world energy, Juin, 2008.
3. C. Ruehl and J. Giljum, *Energy*, 2011, **2030**, 2.
4. J. Tsao, N. Lewis and G. Crabtree, 2006, pp. 1-24.
5. International Renewable Energy Agency, in *Solar Photovoltaics*, 2012, pp. 1-52.
6. International Energy Agency, IEA Publications, Paris, 2010.
7. G. Li, R. Zhu and Y. Yang, *Nat. Photonics*, 2012, **6**, 153-161.
8. P. P. Maharjan, Q. Chen, L. Zhang, O. Adebanjo, N. Adhikari, S. Venkatesan, P. Adhikary, B. Vaagensmith and Q. Qiao, *Phys. Chem. Chem. Phys.*, 2013, **15**, 6856 - 6863.
9. S. Venkatesan, N. Adhikari, J. Chen, E. C. Ngo, A. Dubey, D. W. Galipeau and Q. Qiao, *Nanoscale*, 2014, **6**, 1011-1019.
10. Z. He, C. Zhong, S. Su, M. Xu, H. Wu and Y. Cao, *Nat. Photonics*, 2012, **6**, 591-595.
11. M. O. Reese, A. J. Morfa, M. S. White, N. Kopidakis, S. E. Shaheen, G. Rumbles and D. S. Ginley, *Sol. Energy Mater. Sol. Cells*, 2008, **92**, 746-752.
12. G. Li, V. Shrotriya, J. Huang, Y. Yao, T. Moriarty, K. Emery and Y. Yang, *Nat. Mater.*, 2005, **4**, 864-868.
13. E. C. Chang, C.-I. Chao and R.-H. Lee, *J. Appl. Polym. Sci.*, 2006, **101**, 1919-1924.
14. B. Burkhart, P. P. Khlyabich and B. C. Thompson, *Macromolecules*, 2012, A-I.
15. H. Y. Chen, J. Hou, A. E. Hayden, H. Yang, K. N. Houk and Y. Yang, *Adv. Mater.*, 2010, **22**, 371–375.
16. J. Hou, H. Y. Chen, S. Zhang, G. Li and Y. Yang, *Journal of American Chemical Society*, 2008, **130**, 16144-16145.
17. J. C. Bijleveld, V. S. Gevaerts, D. D. Nuzzo, M. Turbiez, S. G. J. Mathijssen, D. M. d. Leeuw, M. M. Wienk and R. A. J. Janssen, *Adv. Energy Mater.*, 2010, **22**, E242-E246.
18. Y. Liang, Z. Xu, J. Xia, S.-T. Tsai, Y. Wu, G. Li, C. Ray and L. Yu, *Advanced Materials*, 2010, **22**, E135-E138.
19. C. Zhang, S. W. Tong, C. Jiang, E. T. Kang, D. S. H. Chan and C. Zhu, *Applied Physics Letters*, 2008, **92**, 083310.
20. A. G. F. Janssen, T. Riedl, S. Hamwi, H. H. Johannes and W. Kowalsky, *Applied Physics Letters*, 2007, **91**, 073519-073519-073513.
21. J. Y. Kim, S. H. Kim, H.-H. Lee, K. Lee, W. Ma, X. Gong and A. J. Heeger, *Adv. Mater.*, 2006, **18**, 572-576.
22. M. K. Siddiki, J. Li, D. Galipeau and Q. Qiao, *Energy & Environmental Science*, 2010, **3**, 867-883.
23. J. You, L. Dou, K. Yoshimura, T. Kato, K. Ohya, T. Moriarty, K. Emery, C.-C. Chen, J. Gao and G. Li, *Nature communications*, 2013, **4**, 1446.
24. P. Peumans, A. Yakimov and S. R. Forrest, *J. Appl. Phys.*, 2003, **93**, 3693-3723.
25. A. Hadipour, B. de Boer and P. W. M. Blom, *J. Appl. Phys.*, 2007, **102**, 074506-074506.
26. J. Gilot, I. Barbu, M. M. Wienk and R. A. J. Janssen, *Applied Physics Letters*, 2007, **91**, 113520.
27. A. P. Zoombelt, M. Fonrodona, M. M. Wienk, A. B. Sieval, J. C. Hummelen and R. A. Janssen, *Organic letters*, 2009, **11**, 903-906.
28. Y. Xia, L. Wang, X. Deng, D. Li, X. Zhu and Y. Cao, *Applied physics letters*, 2006, **89**, 081106.
29. E. Zhou, S. Yamakawa, K. Tajima, C. Yang and K. Hashimoto, *Chemistry of Materials*, 2009, **21**, 4055-4061.
30. P.-I. Lee, S. L. C. Hsu, J. F. Lee, H. Y. Chuang and P. Lin, *J. Polym. Sci. A Polym. Chem.*, 2011, **49**, 662-670.
31. S.-Y. Jang, B. Lim, B.-K. Yu, J. Kim, K.-J. Baeg, D. Y. Khim and D.-Y. Kim, *Mater. Chem.*, 2011, **21**, 11822-11830.
32. N. Blouin, A. Michaud and M. Leclerc, *Adv. Mater.*, 2007, **19**, 2295-2300.
33. D. Mühlbacher, M. Scharber, M. Morana, Z. Zhu, D. Waller, R. Gaudiana and C. Brabec, *Adv. Mater.*, 2006, **18**, 2884-2889.
34. S. K. Lee, J. M. Cho, Y. Goo, W. S. Shin, J.-C. Lee, W.-H. Lee, I.-N. Kang, H.-K. Shim and S.-J. Moon, *Chemical Communications*, 2011, **47**, 1791-1793.
35. J. Cao, W. Zhang, Z. Xiao, L. Liao, W. Zhu, W. Zuo and L. Ding, *Am. Chem. Soc.*, 2012, A-E.
36. X. Guo, N. Zhou, S. J. Lou, J. Smith, D. B. Tice, J. W. Hennek, R. P. Ortiz, J. T. L. Navarrete, S. Li and J. Strzalka, *Nature Photonics*, 2013.
37. M. M. Wienk, J. M. Kroon, W. J. H. Verhees, J. Knol, J. C. Hummelen, P. A. van Hal and R. A. J. Janssen, *Angew. Chem.*, 2003, **115**, 3493-3497.
38. Y. Yao, C. Shi, G. Li, V. Shrotriya, Q. Pei and Y. Yang, *Applied Physics Letters*, 2006, **89**, 153507-153503.
39. L. G. Kaake, D. Moses and A. J. Heeger, *The Journal of Physical Chemistry Letters*, 2013, **4**, 2264-2268.
40. A. Marti and A. Luque, *Next Generation Photovoltaics-high efficiency through full spectrum utilization*, Institute of Physics Publishing, Bristol and Philadephia, 2004.
41. J. Gilot, M. M. Wienk and R. A. J. Janssen, *Advanced Energy Materials*, 2010, **22**, E67-E71.
42. D. J. D. Moet, P. de Bruyn and P. W. M. Blom, *Applied Physics Letters*, 2010, **96**, 1535041-1535043.
43. J. Y. Kim, K. Lee, N. E. Coates, D. Moses, T.-Q. Nguyen, M. Dante and A. J. Heeger, *Science*, 2007, **317**, 222-225.
44. X. Guo, F. Liu, B. Meng, Z. Xie and L. Wang, *Organic Electronics*, 2010, **11**, 1230-1233.
45. M. K. Siddiki, S. Venkatesan and Q. Qiao, *Phys. Chem. Chem. Phys.*, 2012, **14**, 4682-4686.
46. D. W. Zhao, X. W. Sun, C. Y. Jiang, A. K. K. Kyaw, G. Q. Lo and D. L. Kwong, *Applied Physics Letters*, 2008, **93**, 083305-083305-083303.
47. J. You, C.-C. Chen, Z. Hong, K. Yoshimura, K. Ohya, R. Xu, S. Ye, J. Gao, G. Li and Y. Yang, *Advanced Materials*, 2013, 1-6.
48. S. Sista, Z. Hong, M.-H. Park, Z. Xu and Y. Yang, *Adv. Mater.*, 2010, **22**, E77-E80.
49. C.-H. Chou, W. L. Kwan, Z. Hong, L.-M. Chen and Y. Yang, *Advanced Materials*, 2011, **23**, 1282-1286.

50. D. W. Zhao, X. W. Sun, C. Y. Jiang, A. Kyaw, G. Q. Lo and D. L. Kwong, *Electron Device Letters, IEEE*, 2009, **30**, 490-492.
51. G. Dennler, H.-J. Prall, R. Koeppe, M. Egginger, R. Autengruber and N. S. Sariciftci, *Applied Physics Letters*, 2006, **89**, 073502-073502-073503.
52. D. Cheyns, B. P. Rand and P. Heremans, *Applied Physics Letters*, 2010, **97**, 033301-033303.
53. M. White, D. Olson, S. Shaheen, N. Kopidakis and D. S. Ginley, *Applied Physics Letters*, 2006, **89**, 143517-143517-143513.
54. Z. Xu, L. M. Chen, G. Yang, C. H. Huang, J. Hou, Y. Wu, G. Li, C. S. Hsu and Y. Yang, *Advanced Functional Materials*, 2009, **19**, 1227-1234.
55. S. Kouijzer, S. Esiner, C. H. Frijters, M. Turbiez, M. M. Wienk and R. A. J. Janssen, *Adv. Energy Mater.*, 2012, 1-5.
56. A. Yakimov and S. R. Forrest, *Applied Physics Letters*, 2002, **80**, 1667-1669.
57. A. Hadipour, B. de□Boer, J. Wildeman, F. B. Kooistra, J. C. Hummelen, M. G. R. Turbiez, M. M. Wienk, R. A. J. Janssen and P. W. M. Blom, *Adv. Funct. Mater.*, 2006, **16**, 1897-1903.
58. M. K. Siddiki, S. Venkatesan, M. Wang and Q. Qiao, *Sol. Energy Mater. Sol. Cells*, 2013, **108**, 225-229.
59. B. Minnaert and P. Veelaert, *Materials*, 2012, **5**, 1933-1953.
60. O. Adebanjo, P. P. Maharjan, P. Adhikary, M. Wang, S. Yang and Q. Qiao, *Energy Environ. Sci.*, 2013, **6**, 3150-3170.
61. S. Sista, M.-H. Park, Z. Hong, Y. Wu, J. Hou, W. L. Kwan, G. Li and Y. Yang, *Advanced Materials*, 2010, **22**, 380-383.
62. J. Yang, R. Zhu, Z. Hong, Y. He, A. Kumar, Y. Li and Y. Yang, *Adv. Mater.*, 2011, **23**, 3465-3470.
63. J. Gilot, M. M. Wienk and R. A. J. Janssen, *Applied Physics Letters*, 2007, **90**, 1435121-1435123.
64. V. S. Gevaerts, A. Furlan, M. M. Wienk, M. Turbiez and R. A. J. Janssen, *Adv. Mater.*, 2012, 1-5.
65. L. Dou, J. You, J. Yang, C.-C. Chen, Y. He, S. Murase, T. Moriarty, K. Emery, G. Li and Y. Yang, *Nat. Photonics*, 2012, **6**, 180-185.
66. L. Dou, J. Gao, E. Richard, J. You, C.-C. Chen, K. C. Cha, Y. He, G. Li and Y. Yang, *J. Am. Chem. Soc.*, 2012, **134**, 10071-10079.
67. L. Dou, W.-H. Chang, J. Gao, C.-C. Chen, J. You and Y. Yang, *Adv. Mater.*, 2012, **25**, 825-831.
68. Y. Zhou, C. Fuentes-Hernandez, J. W. Shim, T. M. Khan and B. Kippelen, *Energy Environ. Sci.*, 2012, **5**, 9827-9832.
69. J.-H. Kim, C. E. Song, H. U. Kim, A. C. Grimsdale, S.-J. Moon, W. S. Shin, S. K. Choi and D.-H. Hwang, *Chemistry of Materials*, 2013, **25**, 2722-2732.
70. D. Moet, P. de Bruyn, J. Kotlarski and P. Blom, *Org. Electron.*, 2010, **11**, 1821-1827.
71. J. Yang, J. You, C.-C. Chen, W.-C. Hsu, H.-r. Tan, X. W. Zhang, Z. Hong and Y. Yang, *ACS Nano*, 2011, **5**, 6210-6217.
72. J. Kong, J. Lee, G. Kim, H. Kang, Y. Choi and K. Lee, *Physical Chemistry Chemical Physics*, 2012, **14**, 10547-10555.
73. L. Dou, J. You, J. Yang, C.-C. Chen, Y. He, S. Murase, T. Moriarty, K. Emery, G. Li and Y. Yang, *Nat. Photonics*, 2012.
74. W. Li, A. Furlan, K. H. Hendriks, M. M. Wienk and R. A. Janssen, *Journal of the American Chemical Society*, 2013, **135**, 5529-5532.
75. A. R. bin Mohd Yusoff, W. J. da Silva, H. P. Kim and J. Jang, *Nanoscale*, 2013.
76. J. H. Seo, D.-H. Kim, S.-H. Kwon, M. Song, M.-S. Choi, S. Y. Ryu, H. W. Lee, Y. C. Park, J.-D. Kwon, K.-S. Nam, Y. Jeong, J.-W. Kang and C. S. Kim, *Adv. Mater.*, 2012, **24**, 4523-4527.
77. J. You, L. Dou, Z. Hong, G. Li and Y. Yang, *Progress in Polymer Science*, 2013.
78. T. Ameri, N. Li and C. J. Brabec, *Energy & Environmental Science*, 2013, **6**, 2390-2413.
79. G. Dennler, K. Forberich, T. Ameri, C. Waldauf, P. Denk, C. J. Brabec, K. Hingerl and A. J. Heeger, *Journal of Applied Physics*, 2007, **102**, 123109-123109-123106.
80. P. Boland, K. Lee, J. Dean and G. Namkoong, *Sol. Energy Mater. Sol. Cells*, 2010, **94**, 2170-2175.
81. Y. Min Nam, J. Huh and W. H. Jo, *Sol. Energy Mater. Sol. Cells*, 2011, **95**, 1095-1101.
82. G. Namkoong, P. Boland, K. Lee and J. Dean, *J. Appl. Phys.*, 2010, **107**, 124515-124516.
83. A. Hadipour, B. de Boer and P. W. M. Blom, *Org. Electron.*, 2008, **9**, 617-624.
84. G. Dennler, M. C. Scharber, T. Ameri, P. Denk, K. Forberich, C. Waldauf and C. J. Brabec, *Advanced Materials*, 2008, **20**, 579-583.
85. Y. He, C. Chen, E. Richard, L. Dou, Y. Wu, G. Li and Y. Yang, *J. Mater. Chem.*, 2012, **22**, 13391-13394.
86. F. Wudl, J. C. Hummelen and V. Srdanov, 1996.
87. Z. Bao, A. Dodabalapur and A. J. Lovinger, *Applied Physics Letters*, 1996, **69**, 4108-4110.
88. S. Pillai and M. A. Green, *Sol. Energy Mater. Sol. Cells*, 2010, **94**, 1481-1486.
89. J.-L. Wu, F.-C. Chen, Y.-S. Hsiao, F.-C. Chien, P. Chen, C.-H. Kuo, M. H. Huang and C.-S. Hsu, *ACS Nano*, 2011, **5**, 959-967.
90. B. P. Rand, P. Peumans and S. R. Forrest, *J. Appl. Phys.*, 2004, **96**, 7519-7526.
91. C. Fang-Chung, W. Jyh-Lih, L. Chia-Ling, H. Yi, K. Chun-Hong and M. H. Huang, *Applied Physics Letters*, 2009, **95**, 013305.
92. I. Diukman, L. Tzabari, N. Berkovitch, N. Tessler and M. Orenstein, *Opt. Express*, 2011, **19**, A64-A71.
93. S. Albrecht, S. Schäfer, I. Lange, S. Yilmaz, I. Dumsch, S. Allard, U. Scherf, A. Hertwig and D. Neher, *Org. Electron.*, 2012, **13**, 615-622.
94. J. Kim, G. Kim, Y. Choi, J. Lee, S. H. Park and K. Lee, *J. Appl. Phys.*, 2012, **111**, 114511-114519.
95. M. R. Lilliedal, A. J. Medford, M. V. Madsen, K. Norrman and F. C. Krebs, *Sol. Energy Mater. Sol. Cells*, 2010, **94**, 2018-2031.
96. C. Uhrich, R. Schueppel, A. Petrich, M. Pfeiffer, K. Leo, E. Brier, P. Kilickiran and P. Baeuerle, *Adv. Funct. Mater.*, 2007, **17**, 2991-2999.
97. S. Albrecht, S. Yilmaz, I. Dumsch, S. Allard, U. Scherf, S. Beaupré, M. Leclerc and D. Neher, *Energy Procedia*, 2012, **31**, 159-166.
98. D. Lee, W. K. Bae, I. Park, D. Y. Yoon, S. Lee and C. Lee, *Solar Energy Materials & Solar Cells*, 2010, **95**, 365-368.
99. M. K. Siddiki, S. Venkatesan, D. Galipeau and Q. Qiao, *ACS applied materials & interfaces*, 2013, **5**, 1279-1286.

100.S. Tanaka, K. Mielczarek, R. Ovalle-Robles, B. Wang, D. Hsu and A. Zakhidov, *Applied Physics Letters*, 2009, **94**, 113506-113506-113503.

101.X. Guo, F. Liu, W. Yue, Z. Xie, Y. Geng and L. Wang, *Org. Electron.*, 2009, **10**, 1174-1177.

102.F. Liu and J.-M. Nunzi, *Applied Physics Letters*, 2011, **99**, 063301-063301-063303.

103.T. W. Lee, Y. Chung, O. Kwon and J. J. Park, *Advanced Functional Materials*, 2007, **17**, 390-396.

104.T.-W. Lee, K. Ohyun, K. Mu-Gyeom, P. Sang Hun, C. Jaegwan, K. Sang Yeol, C. Youngsu, J.-Y. Park, E. Han, D. H. Huh, J.-J. Park and P. Lyongsun, *Applied Physics Letters*, 2005, **87**, 231106.

105.J. Meyer, R. Khalandovsky, P. Görrn and A. Kahn, *Advanced Materials*, 2011, **23**, 70-73.

106.M. Kröger, S. Hamwi, J. Meyer, T. Riedl, W. Kowalsky and A. Kahn, *Applied Physics Letters*, 2009, **95**, -.

Graphical abstract